

# Detection of the Yarkovsky effect for main-belt asteroids

David Nesvorný\*, William F. Bottke

*Department of Space Studies, Southwest Research Institute, 1050 Walnut St., Suite 400, Boulder, CO 80302, USA*

Received 19 February 2004; revised 1 April 2004

Available online 9 June 2004

## Abstract

The Yarkovsky effect, a non-gravitational acceleration produced by the anisotropic emission of thermal energy (Öpik, 1951, Proc. Roy. Irish Acad. 54, 165–199), plays an important role in the dynamical evolution of asteroids. Current theoretical models of the Yarkovsky effect, however, rely on a number of poorly known parameters that can only approximate how real asteroids respond to solar heating. To improve this situation, we investigated whether the orbital distribution of the Karin cluster, a  $5.8 \pm 0.2$  Myr old S-type asteroid family (Nesvorný et al., 2002a, Nature 417, 720–722), could be used to determine the rate at which multikilometer main-belt asteroids spread in semimajor axis due to the Yarkovsky effect. Our results indicate that the orbital histories of individual Karin cluster members bear clear signatures of having drifted in semimajor axis drift since their formation. Using numerical methods, we determined the drift speed of  $\approx 70$  Karin cluster members (asteroids 1–6 km in diameter). This is the first time the speed that main-belt asteroids evolve in the semimajor axis due to the non-gravitational effects have been measured. The magnitude of measured speeds is similar to those predicted by theoretical models of the Yarkovsky force. Taken together, our results represent the first direct detection of the Yarkovsky effect for main-belt asteroids, and they validate in significant ways the asteroid thermal models described in the recent literature (e.g., Vokrouhlický, 1999, Astron. Astrophys. 344, 362–366). By comparing the measured drift speeds to those calculated from theoretical models of the Yarkovsky effect, we determined that Karin cluster members do not have surface thermal conductivities  $K$  in excess of  $\sim 0.1 \text{ W m}^{-1} \text{ K}^{-1}$ . Instead, their derived  $K$  values are consistent with the presence of regolith over most/all of their  $\sim 5.8$  Myr lifetimes. This low-conductive regolith layer may be thin because the penetration depth of the diurnal thermal wave is  $\lesssim 5$  cm. The regolith material may have been deposited in the immediate aftermath of the Karin cluster formation event or was produced over time by impacts. Our method also allows us to estimate spin obliquity values for Karin cluster members. We find that members with diameters  $\gtrsim 3.5$ -km are predominantly retrograde rotators, while those  $< 3.5$ -km have obliquities more equally distributed between  $0^\circ$  and  $180^\circ$ . These data may be used to study the spin states of asteroids produced by catastrophic disruption events. Interestingly, we find that a few Karin members have drifted further than predicted by our standard Yarkovsky model. We hypothesize these objects may have: (i) faster drift speeds than predicted by theoretical models, (ii) high albedos ( $\gtrsim 0.3$ ), and/or (iii) densities  $\lesssim 2 \text{ g cm}^{-3}$ .

© 2004 Elsevier Inc. All rights reserved.

*Keywords:* Asteroids; Dynamics

## 1. Introduction

Semimajor axis drift produced by the Yarkovsky effect is the primary mechanism delivering asteroids to resonances that allow them to escape the main belt (e.g., Farinella and Vokrouhlický, 1999; Vokrouhlický and Farinella, 2000; Bottke et al. 2000, 2002; Morbidelli and Vokrouhlický, 2003). To understand the orbital and size distribution of the Near-Earth Asteroids (NEAs), and to determine how often aster-

oids have struck the Earth over time, we need to accurately determine the speed at which asteroids reach the plethora of escape hatches that crisscross the main belt.

Here we report results from a study designed to help us to achieve this goal. Using observations and computer simulations, we have measured, for the first time, the Yarkovsky-induced semimajor axis drifts ( $da/dt$ ) of  $\sim 70$  main-belt asteroids ranging in diameter between 1–6 km. We find that the  $da/dt$  values determined from this work are similar to those predicted by theoretical models of the Yarkovsky effect (e.g., Rubincam et al., 1995, 1998; Farinella et al., 1998; Vokrouhlický, 1998a, 1999). We believe this result has important implications for our understanding of thermal

\* Corresponding author. Fax: (303)-546-9687.

E-mail address: [davidn@boulder.swri.edu](mailto:davidn@boulder.swri.edu) (D. Nesvorný).

effects and the origin of planet-crossing asteroids (see Section 4).

Our findings can also be used to extend results obtained by other researchers. For example, Bottke et al. (2001) showed that some observed structures in the asteroid belt can be explained only if asteroids slowly drift inward and outward in semimajor axis. In our study, we measure the speed of this drift,  $da/dt$ . Chesley et al. (2003) used radar ranging to measure the Yarkovsky effect for 6489 Golevka, a  $\sim 0.5$  km NEA. In our work, we determine the drift speeds for  $\approx 70$  main-belt asteroids ranging from 1 to 6 km in diameter.

To directly measure the strength of the Yarkovsky effect on main-belt asteroids, we use a novel method (described in Section 3) that allows us to compute  $da/dt$  for members of the Karin cluster (Nesvorný et al., 2002a, our Section 2) using existing observations. Our method makes use of the fact that the observed Karin cluster members were nearly instantaneously launched from their parent body  $5.8 \pm 0.2$  Myr ago before drifting into their current positions. The implications of our inferred  $da/dt$  values are discussed in Sections 4 and 5. We argue that the best explanation for the observed semimajor axis distribution of the Karin cluster is evolution via the Yarkovsky effect. Finally, in Section 6, we perform a proof-of-concept numerical simulation to illustrate this conclusion.

## 2. Revised list of the Karin cluster members from new data

Up to now, ejecta from a few tens of major collisions between asteroids (i.e., asteroid families) have been observed in the main belt (e.g., Zappalà et al., 1994). To identify an asteroid family, researchers look for clusters of asteroid positions in the space of the so-called *proper* orbital elements: proper semimajor axis ( $a_P$ ), proper eccentricity ( $e_P$ ), and proper inclination ( $i_P$ ). Proper orbital elements, being more constant over time than instantaneous orbital elements (Milani and Knežević, 1994), provide a dynamical criterion of whether or not a group of bodies has a common ancestor.

The Karin family forms a very compact cluster in proper element space centered around  $a_P = 2.866$  AU,  $e_P = 0.0445$ , and  $i_P = 2.11^\circ$ . Nesvorný et al. (2002a) found that this asteroid family can be best explained if multi-km fragments were launched, as a result of catastrophic impact, from their  $\sim 25$ -km-diameter parent body at velocities  $\lesssim 15$  m s $^{-1}$  (measured ‘at infinity’). The shape of the cluster in  $(a_P, e_P, i_P)$  is then produced if  $-30^\circ \lesssim f \lesssim 30^\circ$  and  $-45^\circ \lesssim \omega + f \lesssim 45^\circ$  (or  $135^\circ \lesssim \omega + f \lesssim 215^\circ$ ), where  $f$  is the true anomaly of the parent body (i.e., the angle between the parent body’s location and the perihelion of its orbit) and  $\omega$  is the parent body’s perihelion argument (i.e., the angle between the perihelion and the ascending node), both measured at the time of the impact event. By numerically integrating 13 member asteroids backwards in time, Nesvorný et al. (2002a) deter-

mined that the breakup event occurred  $5.8 \pm 0.2$  Myr ago. The age is much younger than the inferred age of most observed asteroid families which are hundreds of millions to billions of years old (Marzari et al., 1995; Bottke et al., 2001; Vokrouhlický et al., in preparation; Jedicke et al., 2004; Nesvorný et al., 2004).

For the purpose of the present study, we reexamine the Karin breakup event by augmenting the number of reliably-determined members. To date, only  $\approx 40$  member asteroids are known. These asteroids were taken from the database of 66,089 proper orbital elements available to Nesvorný et al. in 2002 (Knežević et al., 2002).<sup>1</sup> To create an improved list of Karin cluster members, we searched 218,484 asteroid orbits included in Ted Bowell’s ASTORB.DAT database (Bowell et al., 1994), downloaded from the Lowell Observatory web page<sup>2</sup> on 4/18/2003. ASTORB.DAT is a catalog of *osculating* orbital elements. We used the following procedure to calculate proper elements from these osculating orbits.

We selected asteroids with good osculating orbits (those with long observational arcs and several observations) within a box containing the osculating orbits of all known Karin cluster asteroids plus a safety margin (i.e.,  $2.858 \leq a \leq 2.873$  AU,  $e \leq 0.1$ , and  $0.7^\circ \leq i \leq 3.5^\circ$ ). In total, 497 asteroids matched this criteria. We numerically integrated all these orbits backward in time from 2452700.5 JD (March 2, 2003) for 26 myr using the symmetric multistep integrator (Quinlan and Tremaine, 1990) distributed in *Snail* (Nesvorný and Ferraz-Mello, 1997a).<sup>3</sup> This method requires about an order of magnitude more CPU time than the Wisdom–Holman map (Wisdom and Holman, 1991) distributed in the *Swift* code (provided by H.F. Levison and M.J. Duncan) in the low-precision regime, but it is more efficient when high precision is required. Indeed, the high precision of the integrator was essential here.

The initial coordinates and velocities of the planets and asteroids were computed on 2452700.5 JD using JPL Planetary Ephemeris DE405 (Standish, 1990).<sup>4</sup> We corrected them for the Sun–Mercury center of mass and added the mass of Mercury into the Sun’s mass. The seven planets Venus–Neptune were included in the integration. We used the invariant plane of the Solar System as an integration reference frame. The integration time step was 10 days for asteroids (taken as massless test particles) and 2 days for the planets. Relativistic corrections, gravitational perturbations from massive asteroids, and asteroidal thermal forces were neglected. These approximations are further discussed in Section 3.

An on-line low-frequency-pass digital filter was applied to output variables  $a$ ,  $e \exp i\varpi$  and  $i \exp i\Omega$ , where  $e$ ,  $i$ ,  $\varpi$ ,  $\Omega$  are the eccentricity, inclination, perihelion and

<sup>1</sup> <http://hamilton.dm.unipi.it/cgi-bin/astdys/astibo>.

<sup>2</sup> <ftp://ftp.lowell.edu/pub/elgb/astorb.html>.

<sup>3</sup> <http://www.boulder.swri.edu/~davidn/Snail.tar.gz>.

<sup>4</sup> [http://ssd.jpl.nasa.gov/eph\\_info.html](http://ssd.jpl.nasa.gov/eph_info.html).

nodal longitudes, and  $\iota = \sqrt{-1}$ . We used filters A and B defined by Nesvorný and Ferraz-Mello (1997b) that were originally described in Quinn et al. (1991). Our procedure consisted of applying A, A, and B filters sequentially with an increase in sampling by factors of 10, 10, and 3, respectively. This technique increased the initial sampling from  $\sim 4.4$  to  $\sim 1314$  yr. The final signal contains all original Fourier terms with periods larger than  $\sim 5000$  yr; amplitudes of all terms with periods smaller than  $\sim 2500$  yr were suppressed by a factor of  $10^5$ .

The filtered signal was Fourier-analyzed using the Frequency Modified Fourier Transform (FMFT) described by Šidlichovský and Nesvorný (1997).<sup>5</sup> Our method is based on the Modified Fourier Transform developed by Laskar (1993, 1995) but it performs additional corrections designed to improve precision of the determined Fourier terms. We used the FMFT to determine frequencies, amplitudes and phases from digitally filtered  $a$ ,  $e \exp i\varpi$ , and  $i \exp i\Omega$  values for 497 integrated orbits. Each signal was represented by 8192 time outputs that corresponds to a total time span of  $\sim 10.764$  Myr. The 10 Fourier terms with the largest amplitudes were then extracted from those signals.

Four principal sources of error affect the accuracy of the obtained product. The first is the precision of the FMFT itself. Using standard methods (Laskar, 1993), we determined that the FMFT generates relative uncertainties significantly smaller than  $10^{-9}$ ,  $10^{-10}$ , and  $10^{-5}$  in frequencies, amplitudes and phases, respectively. The second source of error is the variability of the frequency decomposition over the signal time span used for the FMFT. To determine the related uncertainty, we carried out the FMFT procedure with twice as many data points; i.e., we used 16,384 time outputs corresponding to a total time span of  $\sim 21.529$  Myr. Comparing this result to our previous one (8192 time outputs), we found that the uncertainties of our original Fourier terms are better than  $10^{-4''}$  yr $^{-1}$  and  $0.1^\circ$  in frequencies and phases, respectively. Uncertainties in amplitudes are typically better than  $10^{-5}$  AU,  $5 \times 10^{-6}$ , and  $5 \times 10^{-6}$  rad for  $a$ ,  $e \exp i\varpi$ , and  $i \exp i\Omega$ , respectively. Both these and the above mentioned uncertainties are acceptable in the context of the current analysis (we discuss this issue further in Section 3).

The remaining two sources of error are the integration error and the uncertainty in the initial orbits and masses. To estimate the integration error, we repeated the analysis using reduced time steps for the numerical integration. The uncertainty in the orbits of asteroids and in the orbits and masses of the planets were obtained from the AstDys node (<http://hamilton.dm.unipi.it/cgi-bin/astdys/astibo>) and from the JPL Planetary Ephemeris DE405. We will estimate and discuss the relevant uncertainties in Sections 3 and 4 together with additional error sources such as the ones introduced by our adopted physical model (i.e., relativistic corrections,

Mercury and massive asteroids excluded from the integration).

We defined the synthetic proper elements and proper frequencies following Šidlichovský and Nesvorný (1997, 1999) and Knežević et al. (2002). We first eliminated the Fourier terms that include secular planetary frequencies  $g_j$  and  $s_j$  (so-called ‘forced’ terms obtained using the FMFT on planetary orbits. The synthetic asteroidal proper (or ‘free’) elements  $a_p, e_p, i_p$  were then defined as amplitudes of the remaining Fourier term of  $a$ ,  $e \exp i\varpi$ , and  $i \exp i\Omega$ , respectively. The frequencies of the latter two terms are the proper perihelion and nodal frequencies, denoted  $g$  and  $s$  in the rest of this paper.

To identify members of the Karin cluster we applied the Hierarchical Clustering Method (HCM, Zappalà et al., 1990)<sup>6</sup> to our synthetic proper elements of 497 asteroids. The HCM starts with an individual asteroid orbit defined in proper elements and identifies bodies in its neighborhood with mutual distances less than a threshold limit ( $d_{\text{cutoff}}$ ). We defined the distance in  $(a_p, e_p, i_p)$  space by:

$$d = na_p \sqrt{C_a(\delta a_p/a_p)^2 + C_e(\delta e_p)^2 + C_i(\delta \sin i_p)^2}, \quad (1)$$

where  $na_p$  is the heliocentric velocity of an asteroid on a circular orbit having semimajor axis  $a_p$ . We also define  $\delta a_p = |a_p^{(1)} - a_p^{(2)}|$ ,  $\delta e_p = |e_p^{(1)} - e_p^{(2)}|$ , and  $\delta \sin i_p = |\sin i_p^{(1)} - \sin i_p^{(2)}|$ . The indices (1) and (2) denote the two bodies in consideration. The values  $C_a$ ,  $C_e$ , and  $C_i$  are constants; we use  $C_a = 5/4$ ,  $C_e = 2$ , and  $C_i = 2$  (Zappalà et al., 1990). Other choices for these constants can be found in the literature, but we find they yield similar results.

The output of HCM is a cluster of asteroids with member bodies connected by a chain in the  $(a_p, e_p, i_p)$  space with the length of each link  $\leq d_{\text{cutoff}}$ . To identify members of the Karin cluster, we tested  $d_{\text{cutoff}}$  values between  $7.5$ – $10$  m s $^{-1}$ . With  $d_{\text{cutoff}} > 10$  m s $^{-1}$ , the algorithm starts to connect background bodies that are unlikely to be members of the Karin cluster. With  $d_{\text{cutoff}} < 7.5$  m s $^{-1}$ , the algorithm fails to connect the small semimajor axis group (located at  $a = 2.861$ – $2.8625$  AU) that we consider an extension of the Karin cluster’s diagonally-shaped structure in  $a_p, e_p$  space (see Fig. 1). In the end, we adopted  $d_{\text{cutoff}} = 7.5$  m s $^{-1}$ , which yielded 97 Karin cluster members. We found that with  $d_{\text{cutoff}} > 7.5$  m s $^{-1}$  the HCM adds bodies that are later excluded from the list because they do not show alignment of  $\varpi$  and  $\Omega$  at  $t = -5.8$  Myr (see below). It is thus just a matter of convenience to use more restrictive  $d_{\text{cutoff}} = 7.5$  m s $^{-1}$ .

To remove interlopers from our cluster, we required Karin cluster members to have their proper  $\varpi$  and  $\Omega$  aligned to within  $\pm 60^\circ$  of the proper  $\varpi$  and  $\Omega$  values of (832) Karin after 5.8 Myr of backwards integration (i.e.,  $t = -5.8$  Myr). Note that real cluster members, by necessity, had nearly identical orbits when the Karin cluster formed  $\sim 5.8$  ago (Nesvorný et al., 2002a). We allowed for a  $\pm 60^\circ$  spread in

<sup>5</sup> <http://www.boulder.swri.edu/~davidn/fmft/fmft.html>.

<sup>6</sup> <http://www.boulder.swri.edu/~davidn/family/family.html>.

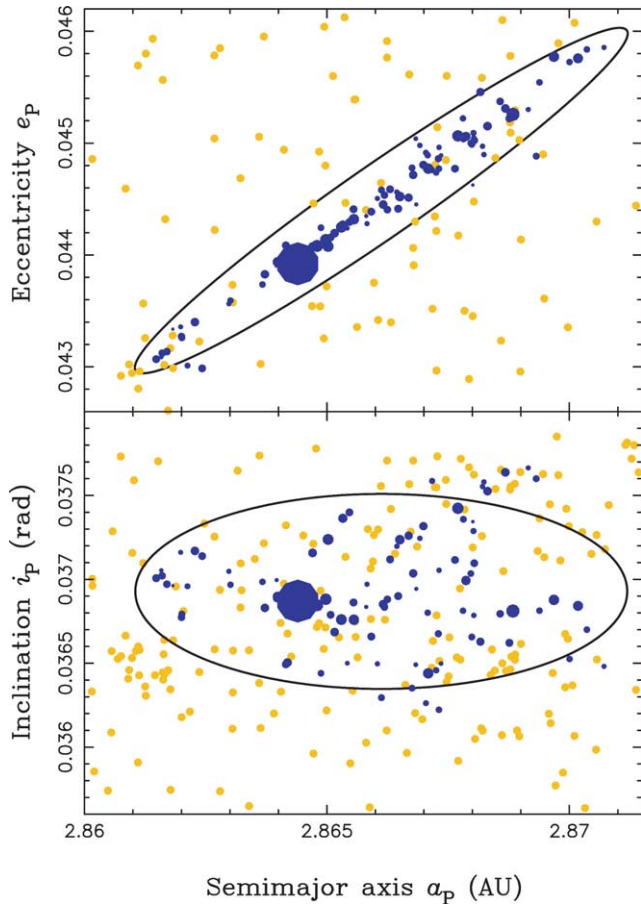


Fig. 1. Proper orbital elements of ninety Karin cluster members: (top)  $a_p$ ,  $e_p$ , and (bottom)  $a_p$ ,  $i_p$ . The size of each blue symbol is proportional to the diameter of a cluster member. Golden dots indicate the background bodies in the Koronis family. The black ellipses show the proper orbital elements of test bodies launched with  $15 \text{ m s}^{-1}$  speed from  $a_p = 2.8661 \text{ AU}$ ,  $e_p = 0.04449$  and  $i_p = 0.03692$ , assuming  $f = 30^\circ$ , and  $\omega + f = 45^\circ$  (Nesvorný et al., 2002a).

$\varpi$  and  $\Omega$  because the past orbital histories of Karin cluster members have yet to be corrected for thermal effects.

We used the FMFT to determine proper  $\varpi$  and  $\Omega$  for each asteroid. The algorithm is exactly the same as the one we used to define  $a_p$ ,  $e_p$ ,  $i_p$ , only this time we ran the FMFT over the time intervals  $(t_j, t_j + \Delta t)$ , where  $t_j \sim 13,140 \times j \text{ yr}$ ,  $j = 1, \dots, 1000$ , and  $\Delta t \sim 10.764 \text{ Myr}$ . The proper perihelion and nodal longitudes at time  $t$ , denoted as  $\varpi_p(t)$  and  $\Omega_p(t)$  in the following text, are the phases of the proper Fourier terms of  $e \exp i\varpi$  and  $i \exp i\Omega$  determined over the interval  $(t_j, t_j + \Delta t)$ , where  $t_j = t$ .

We defined  $\Delta\varpi_{p,j} = \varpi_{p,j} - \varpi_{p,1}$  and  $\Delta\Omega_{p,j} = \Omega_{p,j} - \Omega_{p,1}$ , where  $\varpi_{p,j}$  and  $\Omega_{p,j}$ ,  $j = 1, \dots, 97$ , are the proper perihelion and nodal longitudes, respectively, of our 97 asteroids, and  $j = 1$  refers to (832) Karin. Orbital alignment occurs when  $\Delta\varpi_{p,j} \sim 0$  and  $\Delta\Omega_{p,j} \sim 0$  for most  $j$  values at a chosen epoch.

We found that only seven bodies from our original list of 97 have  $\Delta\varpi_p > 60^\circ$  or  $\Delta\Omega_p > 60^\circ$  at  $t = -5.8 \text{ Myr}$ . Among these seven determined interlopers were (158) Ko-

ronis and (4507) 1990 FV. The case of (158) Koronis was clear: its  $\varpi_p$  and  $\Omega_p$  were offset by  $134.9^\circ$  and  $166.4^\circ$  from  $\varpi_p$  and  $\Omega_p$  of (832) Karin at  $t = -5.8 \text{ Myr}$ , and they did not become aligned at any time within the past 26 Myr. The same goes for (4507) 1990 FV, for which  $\varpi_p$  and  $\Omega_p$  were offset by  $128.0^\circ$  and  $23.8^\circ$  from  $\varpi_p$  and  $\Omega_p$  of (832) Karin at  $t = -5.8 \text{ Myr}$ . The fact that (4507) 1990 FV is now identified as an interloper is interesting because this body was originally believed, by its  $a_p$ ,  $e_p$ ,  $i_p$  value alone, to be the second-largest Karin cluster member (Nesvorný et al., 2002a).

Figure 1 shows the proper element distribution of the remaining 90 members of the Karin cluster. Their proper orbital elements and proper frequencies are listed in Table 1. Figure 2 shows  $\Delta\varpi_{p,j}(t)$  and  $\Delta\Omega_{p,j}(t)$ ,  $j = 1, \dots, 90$ , for  $-10^7 \leq t \leq 0$  years. These results confirm those obtained by Nesvorný et al. (2002a). They also provide additional evidence for the orbital alignment of Karin members at  $t \sim -5.8 \text{ Myr}$ .

Using the methods described by Nesvorný et al., we can use the 34 numbered asteroids from our expanded list of cluster members to slightly revise the age of the Karin cluster. The orbits for these objects have better than  $10^{-6} \text{ AU}$ ,  $5 \times 10^{-7}$  and  $5 \times 10^{-5} \text{ deg}$   $1\text{-}\sigma$  uncertainties in  $a$ ,  $e$ , and  $i$ , respectively.<sup>7</sup> We find that at  $t = -5.7 \text{ Myr}$ , the arithmetic means of  $\Delta\varpi_p$  and  $\Delta\Omega_p$  for this subset are  $\langle\Delta\varpi_p\rangle = 10.8^\circ$  and  $\langle\Delta\Omega_p\rangle = 13.6^\circ$ , respectively. These values correspond to the lowest values of  $\langle\Delta\varpi_p\rangle$  and  $\langle\Delta\Omega_p\rangle$  for any  $t$ . Our revised Karin cluster age,  $\sim 5.7 \text{ Myr}$ , is similar to the  $5.8 \pm 0.2 \text{ Myr}$  age determined by (Nesvorný et al., 2002a). We will further improve this estimate in the next section.

### 3. Past orbital histories of member asteroids

Figure 2 shows that orbits of the Karin cluster members were not *exactly* identical at  $t \sim -5.7 \text{ Myr}$ . For example, the individual orbits were located in a number of slightly rotated planes because  $\Delta\Omega_{p,j}$  were spread over  $\pm 40^\circ$ . Similarly, the perihelia of the individual orbits were also slightly rotated with respect to each other at  $t \sim -5.7 \text{ Myr}$  because the  $\Delta\varpi_{p,j}$  values were spread over  $\pm 40^\circ$ . These differences could not have been a consequence of the breakup event itself.

We know from the structure of the Karin cluster in  $(a_p, e_p, i_p)$  space that the ejection speeds  $\delta V$  (measured at ‘infinity’) of individual fragments were  $\lesssim 15 \text{ m s}^{-1}$ . Assuming  $\delta V \lesssim 15 \text{ m s}^{-1}$ , we calculate from the Gauss equations (e.g., Murray and Dermott, 1999, p. 54) that the generated fragments should initially have had  $\Delta\Omega_p \lesssim 0.9^\circ$  and  $\Delta\varpi_p \lesssim 1.1^\circ$ . In contrast, the  $\Delta\Omega_p$  and  $\Delta\varpi_p$  values of Karin cluster members observed in Fig. 2 have a much wider spread at  $t \sim -5.7 \text{ Myr}$ .

<sup>7</sup> <http://hamilton.dm.unipi.it/cgi-bin/astdys/astibo>.

Table 1  
Proper orbits of the Karin cluster members

Number	Name	$H$ (mag)	$a_p$ (AU)	$e_p$	$i_p$ (rad)	$g$ " yr <sup>-1</sup>	$s$ " yr <sup>-1</sup>	$\log_{10} \gamma$ $\gamma$ in yr <sup>-1</sup>
832	Karin	11.18	2.86440	0.043921	0.036862	70.8096	-65.4047	-6.18
7719	1997 GT36	14	2.86770	0.045065	0.037415	71.0864	-65.6650	-6.21
10783	1991 RB9	13.9	2.86480	0.044081	0.036837	70.8457	-65.4379	-6.16
11728	Einer	14.2	2.86556	0.044320	0.036751	70.9150	-65.4992	-5.99
13765	Nansmith	14.2	2.86968	0.045773	0.036869	71.2814	-65.8336	-6.03
13807	1998 XE13	13.7	2.86883	0.045257	0.036803	71.2059	-65.7578	-6.18
15649	6317 P-L	14.6	2.86418	0.043948	0.036496	70.8027	-65.3954	-6.25
16706	Svojsik	14.9	2.86200	0.043271	0.036766	70.6051	-65.2197	-6.16
20089	1994 PA14	14.9	2.86170	0.043136	0.036963	70.5731	-65.1924	-6.22
20095	1994 PG35	14.2	2.86709	0.044772	0.036432	71.0601	-65.6241	-6.18
23054	1999 XE42	15.2	2.86938	0.045543	0.036805	71.2553	-65.8053	-6.20
23338	2809 P-L	15.1	2.86781	0.045038	0.037349	71.0979	-65.6726	-6.22
26970	1997 SE2	15.3	2.86725	0.044737	0.036450	71.0734	-65.6338	-6.18
28271	1999 CK16	14.3	2.87018	0.045758	0.036834	71.3260	-65.8675	-6.05
33143	1998 DJ7	14.6	2.86831	0.045152	0.037517	71.1370	-65.7089	-6.19
34312	2000 QO188	14.9	2.86858	0.045373	0.036787	71.1835	-65.7435	-6.17
40510	1999 RU87	14.6	2.86868	0.045310	0.037629	71.1671	-65.7388	-6.11
40782	1999 TX26	14.7	2.86699	0.044805	0.037308	71.0257	-65.6081	-6.27
40789	1999 TW31	14.8	2.86148	0.043069	0.036999	70.5530	-65.1745	-6.19
40921	1999 TR171	14.8	2.86876	0.045221	0.036613	71.2039	-65.7531	-6.23
41307	1999 XA149	15.7	2.86604	0.044505	0.036488	70.9663	-65.5424	-6.16
43032	1999 VR26	14.6	2.86616	0.044451	0.036844	70.9652	-65.5441	-6.16
47640	2000 CA30	14	2.86498	0.044137	0.036873	70.8604	-65.4517	-6.15
48369	4153 T-2	14.8	2.86647	0.044414	0.036892	70.9899	-65.5634	-6.16
50715	2000 EV136	14.8	2.86591	0.044387	0.036651	70.9493	-65.5273	-6.09
51068	2000 GW156	15.2	2.86367	0.043736	0.036977	70.7430	-65.3472	-6.19
51089	2000 GO178	15.2	2.87036	0.045838	0.036692	71.3460	-65.8840	-5.76
51923	2001 QD95	15.6	2.86731	0.044962	0.037045	71.0630	-65.6391	-6.20
52009	2002 EU146	15.8	2.86198	0.043358	0.037152	70.5930	-65.2170	-6.18
55124	2001 QU170	15.4	2.86704	0.044915	0.036254	71.0625	-65.6280	-6.18
55434	2001 TZ66	15.6	2.86824	0.044898	0.037572	71.1266	-65.6939	-5.99
55852	1996 TS34	16.1	2.86158	0.043087	0.037045	70.5605	-65.1818	-6.16
56285	1999 LJ3	15.9	2.86542	0.044239	0.036492	70.9103	-65.4901	-6.15
57735	2001 UQ159	14.9	2.86625	0.044405	0.036872	70.9713	-65.5480	-6.16
	1994 EX	14.39	2.86650	0.044522	0.037228	70.9840	-65.5657	-6.17
	1995 EC5	15.26	2.86781	0.045221	0.036804	71.1152	-65.6852	-6.16
	1995 TH10	15.05	2.86730	0.044861	0.036668	71.0719	-65.6388	-6.16
	1995 UN13	14.7	2.86669	0.044513	0.037251	70.9987	-65.5774	-6.14
	1998 SQ81	14.11	2.86502	0.044077	0.037229	70.8532	-65.4485	-6.16
	1999 TB129	15.22	2.87000	0.045725	0.036517	71.3198	-65.8581	-6.24
	1999 TV145	14.63	2.86228	0.043400	0.037161	70.6177	-65.2384	-6.22
	1999 UJ18	15.7	2.86298	0.043564	0.037039	70.6814	-65.2932	-6.18
	1999 VM71	15.09	2.86612	0.044581	0.036287	70.9796	-65.5528	-6.23
	1999 VW121	15.7	2.87071	0.045855	0.036473	71.3847	-65.9123	-6.26
	1999 VV155	15.63	2.86644	0.044562	0.037189	70.9802	-65.5634	-6.18
	1999 WZ18	16.72	2.86182	0.043337	0.036954	70.5853	-65.2076	-6.20
	1999 XD38	15.04	2.86201	0.043261	0.036784	70.6050	-65.2196	-6.17
	1999 XE68	14.49	2.86533	0.044268	0.037355	70.8772	-65.4747	-6.14
	2000 AW87	14.28	2.86437	0.043869	0.036868	70.8067	-65.4009	-6.15
	2000 CH101	16.62	2.86801	0.044626	0.037335	71.1112	-65.6710	-6.23
	2000 DU31	15.61	2.86821	0.044972	0.037545	71.1256	-65.6949	-5.85
	2000 DH36	15.11	2.86799	0.044990	0.036648	71.1334	-65.6911	-6.16
	2000 FM55	14.72	2.86816	0.045457	0.036620	71.1540	-65.7205	-5.60
	2000 HN72	14.57	2.86470	0.044076	0.037149	70.8284	-65.4276	-6.17
	2000 QJ18	14.85	2.86804	0.045025	0.037088	71.1251	-65.6906	-5.98
	2000 QM81	14.82	2.86507	0.044157	0.036780	70.8717	-65.4602	-6.15
	2000 SX40	15.6	2.86803	0.045048	0.036777	71.1337	-65.6944	-6.06
	2000 SR228	16.2	2.86684	0.044452	0.036935	71.0211	-65.5898	-6.14
	2000 UV4	14.78	2.86415	0.044086	0.036486	70.8013	-65.3980	-6.25
	2000 UE79	14.83	2.86764	0.044772	0.037107	71.0879	-65.6541	-6.20

(continued on next page)

Table 1 (continued)

Number	Name	$H$ (mag)	$a_p$ (AU)	$e_p$	$i_p$ (rad)	$g$ " yr <sup>-1</sup>	$s$ " yr <sup>-1</sup>	$\log_{10} \gamma$ $\gamma$ in yr <sup>-1</sup>
	2000 VE21	15.34	2.86802	0.045091	0.037279	71.1185	-65.6896	-6.18
	2000 YQ59	14.11	2.86530	0.044248	0.036752	70.8923	-65.4790	-6.20
	2001 FB69	14.82	2.86243	0.042986	0.037130	70.6272	-65.2346	-6.16
	2001 QF18	14.44	2.86787	0.045059	0.036985	71.1126	-65.6806	-6.20
	2001 QP94	14.91	2.86160	0.043123	0.037013	70.5632	-65.1845	-6.18
	2001 QZ160	15.09	2.86675	0.044779	0.036343	71.0339	-65.6024	-6.19
	2001 RB118	14.65	2.86372	0.043827	0.036822	70.7459	-65.3501	-6.10
	2001 SO88	15.35	2.86717	0.044759	0.037578	71.0327	-65.6156	-6.19
	2001 SX166	15.44	2.86212	0.043011	0.036950	70.6075	-65.2170	-6.18
	2001 SE168	14.81	2.86630	0.044587	0.037111	70.9707	-65.5556	-6.17
	2001 SH169	15.15	2.86797	0.044999	0.037026	71.1205	-65.6855	-6.17
	2001 SG298	15.92	2.86683	0.045040	0.036483	71.0392	-65.6158	-6.17
	2001 SH304	15.61	2.86692	0.044980	0.037236	71.0233	-65.6104	-6.17
	2001 TW49	14.81	2.86397	0.043942	0.036878	70.7745	-65.3771	-6.17
	2001 UA133	15.97	2.86735	0.044890	0.036490	71.0823	-65.6458	-6.17
	2001 VU113	15.26	2.86708	0.044892	0.036793	71.0496	-65.6234	-6.16
	2001 WG20	15.74	2.86915	0.045301	0.037656	71.2073	-65.7703	-6.06
	2001 XU92	14.68	2.86678	0.044716	0.037027	71.0154	-65.5939	-6.16
	2001 XD232	15.09	2.86932	0.044884	0.037591	71.2198	-65.7671	-6.00
	2002 AL107	16.2	2.86581	0.044348	0.036827	70.9347	-65.5167	-5.56
	2002 AO172	14.92	2.86619	0.044535	0.036826	70.9687	-65.5491	-6.17
	2002 CV38	15.7	2.86583	0.044280	0.036962	70.9317	-65.5139	-5.95
	2002 CL81	15.24	2.86301	0.043593	0.036959	70.6868	-65.2974	-6.05
	2002 CX104	14.81	2.86555	0.044409	0.036854	70.9122	-65.5007	-6.13
	2002 CV120	15.2	2.86731	0.044772	0.036215	71.0854	-65.6416	-6.19
	2002 SQ20	15.14	2.86488	0.044244	0.036432	70.8659	-65.4538	-6.17
	2002 TH97	16.24	2.86396	0.043904	0.036987	70.7690	-65.3729	-6.16
	2002 TJ250	14.6	2.86516	0.044195	0.036678	70.8821	-65.4684	-6.19
	2002 TO257	14.81	2.86546	0.044295	0.037391	70.8879	-65.4845	-6.22
	2247 T-2	14.33	2.86398	0.043938	0.036889	70.7739	-65.3767	-6.16

The columns are: number and name of an asteroid,<sup>8</sup> its absolute magnitude ( $H$ ), proper semimajor axis ( $a_p$ ), proper eccentricity ( $e_p$ ), proper inclination ( $i_p$ , measured with respect to the invariable plane of planets), proper perihelion frequency ( $g$ ), proper nodal frequency ( $s$ ), and estimate of the maximum Lyapunov exponent at  $t = 2.6 \times 10^7$  yr ( $\gamma$ ).

We believe the most plausible explanation for this mismatch is semimajor axis drift of Karin cluster members over the past  $\sim 5.7$  Myr. The most likely candidate mechanisms to produce this drift are Yarkovsky thermal forces and/or encounters with (1) Ceres. Other alternatives do not appear to work: (i) the asteroid's orbital uncertainty is too small to matter;<sup>9</sup> (ii) uncertainties in the orbits and masses of the planets produce negligible differential effects on the

members'  $\Delta\Omega_p$  and  $\Delta\varpi_p$  values because all Karin cluster members have similar orbits ( $2.861 \text{ AU} \lesssim a_p \lesssim 2.871 \text{ AU}$ ,  $0.043 \lesssim e_p \lesssim 0.046$ , and  $0.0363 \lesssim i_p \lesssim 0.0375$ ); (iii) the direct effect of the Yarkovsky force on the apsidal and nodal rates is negligible in the current context (Spitale and Greenberg, 2002); (iv) the integration errors are  $< 1^\circ$  in  $\Omega$  and  $\varpi$  at  $t \sim -5.7$  Myr; (v) the chaos influencing asteroid orbits at the location of the Karin cluster is unimportant on  $< 10$  Myr timescales;<sup>10</sup> (vi) gravitational perturbations by

<sup>8</sup> Since the original compilation of this table five asteroids become numbered: (64165) 2001 TW49, (69009) 2002 TJ250, (69880) 1998 SQ81, (71003) 1999 XD38, and (71031) 1999 XE68.

<sup>9</sup> For example, the numbered Karin cluster members have  $\sigma_a = 10^{-6}$  AU,  $\sigma_e = 5 \times 10^{-7}$  and  $\sigma_i = 5 \times 10^{-5}$  deg uncertainties in  $a$ ,  $e$ , and  $i$ , respectively. The effect of these uncertainties on  $\Delta\Omega_p$  can be estimated from

$$(\Delta\Omega_p)^2 = \left(\frac{\partial s}{\partial a}\right)^2 \sigma_a^2 \tau^2 + \left(\frac{\partial s}{\partial e}\right)^2 \sigma_e^2 \tau^2 + \left(\frac{\partial s}{\partial i}\right)^2 \sigma_i^2 \tau^2,$$

where  $\partial s/\partial a \approx -70'' \text{ yr}^{-1} \text{ AU}^{-1}$ ,  $\partial s/\partial e \approx -34'' \text{ yr}^{-1}$ , and  $\partial s/\partial i \approx 0$  at the Karin cluster location, and  $\tau \approx 5.7$  Myr. By far the largest term in the above expression is the first one. This term produces about  $0.1^\circ$  uncertainty in  $\Delta\Omega_p$  at  $t = -5.7$  Myr. In contrast, observed  $\langle \Delta\Omega_p \rangle = 13.6^\circ$ , i.e., about two magnitudes larger. The same argument applies to  $\Delta\varpi_p$ .

<sup>10</sup> We have determined the Lyapunov times for an exponential stretching of nearby orbits for all 497 integrated bodies (Oseledec, 1968; Benettin et al., 1976). Only 2002 CJ4 and 2002 EP136 (not members of the Karin cluster) happen to have the Lyapunov time shorter than  $10^5$  yr probably due to the three-body resonance  $17\lambda_J - 12\lambda_S - 5\lambda = 0$  (located at  $a \sim 2.8727$  AU), where  $\lambda_J$ ,  $\lambda_S$ , and  $\lambda$  are mean longitudes of Jupiter, Saturn and asteroid, respectively (Nesvorný and Morbidelli, 1998). Only about 10% of the integrated orbits have the Lyapunov time shorter than  $10^6$  yr. Theoretically, the effects of chaos on these orbits could affect the evolution of  $\Omega$  and  $\varpi$  on Myr timescales. In practice, however, it is well known that the stretching affects of the three-body resonances are large in  $\lambda$  but are much smaller in other dimensions represented by secular angles  $\Omega$  and  $\varpi$ . This is why the effects of chaos on evolution tracks in Fig. 2 are negligible. We confirmed this by numerical integrations using reduced integration time steps.

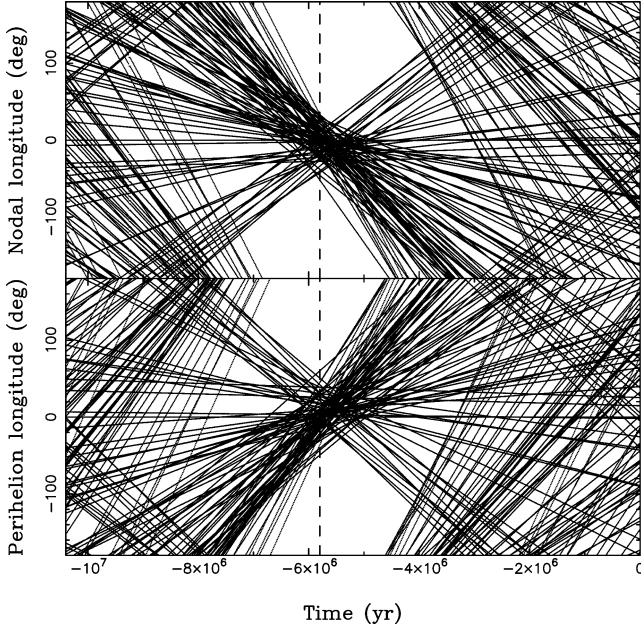


Fig. 2. The convergence of angles at  $t \approx 5.8$  Myr confirms that the Karin cluster was created by a parent asteroid breakup at that time (Nesvorný et al., 2002a, 2002b, 2002c). The plot shows past orbital histories of the ninety members of the Karin cluster: (top) proper nodal longitude  $\Omega_P$  and (bottom) proper perihelion longitude  $\varpi_P$ . Values of these angles relative to (832) Karin are shown. At  $t = -5.8$  Myr (broken vertical line), the nodal longitudes and perihelion arguments of all ninety asteroids were nearly the same. Thus, at  $t \approx -5.8$  Myr, all orbits were nearly identical strongly suggesting that the breakup event occurred at that time.

Mercury have negligible differential effects on  $\Delta\Omega_P$  and  $\Delta\varpi_P$ ; (vii) *direct* effects of (1) Ceres and other asteroids on  $\Delta\Omega_P$  and  $\Delta\varpi_P$  can be also ignored (Vokrouhlický et al., 2001; Nesvorný et al., 2002b; Carruba et al., 2003);<sup>11</sup> (viii) relativistic effects accelerate the rotations of the members'  $\varpi_P$  values by  $\approx 4.5^\circ$  per 5.8 Myr. The differential relativistic effects on  $\Delta\varpi_P$  are negligible. We confirmed this using a numerical simulation where we accounted for relativistic corrections using the formalism described by Quinn et al. (1991).

We now explain how the orbital paths recorded in Fig. 2 can be used to calculate the semimajor axis drift of Karin cluster members. We assume that Karin's family members were generated by the parent body breakup at  $t = -\tau$ , where  $\tau$  is the age of the Karin cluster. Moreover, we assume that the fragments'  $\delta\Omega_P$  and  $\delta\varpi_P$  values produced by ejection velocities  $\delta V$  at  $t = -\tau$  were small ( $\lesssim 1^\circ$  in our case). At  $t > -\tau$ ,  $\Omega_P$  and  $\varpi_P$  rotated due to gravitational planetary perturbations with proper frequencies  $s = \Omega_P$  and  $g = \varpi_P$  that depend on  $a_P$ ,  $e_P$ , and  $i_P$  of a fragment's orbit. For each fragment's orbit, we assume that its proper semimajor axis

drifted with constant speed  $\dot{a}_P$  from  $t = -\tau$  to  $t = 0$ , with the  $s$  and  $g$  frequencies evolving accordingly. At  $t = 0$  (i.e., now), the values of proper secular angles are:

$$\begin{aligned}\Omega_P(t=0) &= \Omega_P^* + s^*\tau + \frac{1}{2} \frac{\partial s}{\partial a_P} \dot{a}_P \tau^2, \\ \varpi_P(t=0) &= \varpi_P^* + g^*\tau + \frac{1}{2} \frac{\partial g}{\partial a_P} \dot{a}_P \tau^2,\end{aligned}\quad (2)$$

where  $\Omega_P^*$  and  $\varpi_P^*$  are the initial values at  $t = -\tau$ ,  $s^*$  and  $g^*$  are the proper frequencies of the initial orbit,<sup>12</sup> and  $\partial s/\partial a_P$  and  $\partial g/\partial a_P$  define how frequencies change with  $a_P$ . Using an analytic perturbation theory (Milani and Knežević, 1994), we calculate that  $\partial s/\partial a_P = -70.0 \pm 0.2$  arcsec yr<sup>-1</sup> AU<sup>-1</sup> and  $\partial g/\partial a_P = 94.3 \pm 0.6$  arcsec yr<sup>-1</sup> AU<sup>-1</sup> at the location of the Karin cluster, where the main source of uncertainty comes from the spread of the Karin cluster in  $a_P$  and the fact that  $|\partial s/\partial a_P|$  and  $|\partial g/\partial a_P|$  are larger for larger  $a_P$ . To simplify the procedure, we assume that  $\partial s/\partial a_P = -70.0$  arcsec yr<sup>-1</sup> AU<sup>-1</sup> and  $\partial g/\partial a_P = 94.3$  arcsec yr<sup>-1</sup> AU<sup>-1</sup> for all Karin cluster members. This assumption introduces  $\lesssim 1\%$  uncertainty into our results.

Because we neglect thermal effects in our backward integration,  $\dot{a}_P = 0$ . For this reason,  $\Omega_P$  and  $\varpi_P$  move back towards their original values with constant speeds  $-s$  and  $-g$ , where  $s$  and  $g$  are the proper secular frequencies shown in Table 1. At  $t = -(\tau + \Delta t)$ , the values of secular angles are:

$$\begin{aligned}\Omega_P(-\tau - \Delta t) &= \Omega_P^* - \frac{1}{2} \frac{\partial s}{\partial a_P} \delta a_P \tau - s \Delta t, \\ \varpi_P(-\tau - \Delta t) &= \varpi_P^* - \frac{1}{2} \frac{\partial g}{\partial a_P} \delta a_P \tau - g \Delta t,\end{aligned}\quad (3)$$

where  $\delta a_P = \dot{a}_P \tau$  is the total semimajor axis drift over  $\tau$ .

We follow  $\Omega_P$  and  $\varpi_P$  of body  $j$  and calculate the angular difference with respect to the orbit of a reference object:

$$\begin{aligned}\Delta\Omega_{P,j}(-\tau - \Delta t) &= \Omega_{P,j}^* - \Omega_{P,1}^* - \frac{1}{2} \frac{\partial s}{\partial a_P} (\delta a_{P,j} - \delta a_{P,1}) \tau - (s_j - s_1) \Delta t, \\ \Delta\varpi_{P,j}(-\tau - \Delta t) &= \varpi_{P,j}^* - \varpi_{P,1}^* - \frac{1}{2} \frac{\partial g}{\partial a_P} (\delta a_{P,j} - \delta a_{P,1}) \tau - (g_j - g_1) \Delta t,\end{aligned}\quad (4)$$

where indexes 1 and  $j$  denote quantities of the reference ((832) Karin in our case) and body  $j$ , respectively. There are three terms in the first row of Eq. (4): (i)  $\Omega_{P,j}^* - \Omega_{P,1}^*$  is the proper nodal longitude difference caused by the ejection speeds  $\delta V$ , (ii)  $(1/2)(\partial s/\partial a_P)(\delta a_{P,j} - \delta a_{P,1})\tau$  is the effect of the differential rotations of  $\Omega_{P,j}$  over  $\tau$  due to the semimajor axis drift, and (iii)  $(s_j - s_1)\Delta t$  is a correction that vanishes for  $\Delta t = 0$ . The same terms appear in the

<sup>11</sup> Encounters with (1) Ceres and other large asteroids in the main belt produce small perturbations on  $a_P$  (Vokrouhlický et al., 2001; Nesvorný et al., 2002b; Carruba et al., 2003) that may lead to significant cumulative evolutions in frequencies and proper angles over the Karin cluster age. We will estimate the magnitude of these evolutions in Section 5.

<sup>12</sup> We assume that  $e_P$  and  $i_P$  of fragments are constant and equal to the ones generated at  $t = -\tau$  by the breakup event. This is a good approximation for the Yarkovsky effect because  $e_P$  and  $i_P$  of Karin cluster members are small (Bottke et al., 2000; Spitale and Greenberg, 2002).

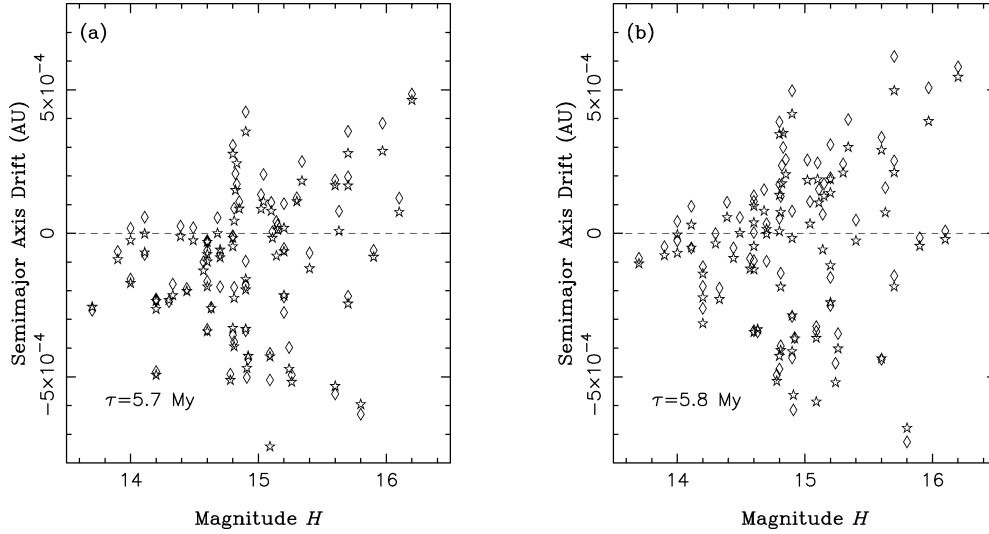


Fig. 3. Semimajor axis drifts  $\Delta a_p$  for 70 Karin cluster asteroids that we determined for: (a)  $\tau = 5.7$  Myr, and (b)  $\tau = 5.8$  Myr. The diamonds and stars denote  $\Delta a_p$  computed from  $\Delta \Omega_p$  and  $\Delta \varpi_p$ , respectively. Neighbor symbols correspond to these two measurements for an individual object.

second row of Eq. (4) that describes the differential effect of  $\delta a_{p,j}$  on  $\varpi_{p,j}$ . By solving these last two equations for  $\Delta a_{p,j} = \delta a_{p,j} - \delta a_{p,1}$ , we obtain the values of  $\Delta a_p$  that are required to compensate for the observed  $\Delta \Omega_p$  and  $\Delta \varpi_p$  of individual orbits at  $t \sim -5.7$  Myr (e.g., Fig. 2).

The two determinations of  $\Delta a_p$  obtained from  $\Delta \Omega_p$  and  $\Delta \varpi_p$  are independent, allowing us to use them to pin down the precise age of the Karin cluster. We assume that  $\Omega_{p,j}^* - \Omega_{p,1}^* = 0$  and  $\varpi_{p,j}^* - \varpi_{p,1}^* = 0$  for all  $j$ . We then calculate  $\chi(t) = \sum_{j=2}^N |\Delta a_{p,j}^{\Omega} - \Delta a_{p,j}^{\varpi}| / (N - 1)$  as a function of time, where  $\Delta a_{p,j}^{\Omega}$  and  $\Delta a_{p,j}^{\varpi}$  are the two measurements of drift speed from  $\Omega_{p,j}$  and  $\varpi_{p,j}$ , respectively (Eq. (4)), and  $N$  is the considered number of Karin cluster members. We proceed by iterations to determine the minimum of  $\chi(t)$ . In the first step, we assume that  $\tau_1 = -5.7$  Myr and solve for  $\Delta t_1$ . Next, we calculate  $\tau_2 = \tau_1 + \Delta t_1$  and solve for new  $\Delta t_2$ . This procedure converges quickly. When  $\Delta t \sim 0$ , the computed  $\tau$  value is the Karin cluster's age that provides the best fit for our model and minimizes the differences between  $\Delta a_{p,j}^{\Omega}$  and  $\Delta a_{p,j}^{\varpi}$ .

To determine  $\tau$ , we used the orbits of 34 numbered Karin cluster members. Our results show that  $\tau = 5.75 \pm 0.05$  Myr and  $\chi(-5.75 \text{ Myr}) = 1.6 \times 10^{-5}$  AU. The determined age is nearly identical to the one found by Nesvorný et al. (2002a). We consider the value of  $\chi$  for  $\tau = -5.75$  Myr satisfactory because the semimajor axis drift rates measured by our technique are up to one order of magnitude larger. This value of  $\chi$  corresponds to  $\sim 1^\circ$  uncertainties in angles  $\Delta \Omega_{p,j}^*$  and  $\Delta \varpi_{p,j}^*$ , which can be easily explained by  $\delta V \sim 15 \text{ m s}^{-1}$  or some combination of effects ignored by our other assumptions. The error bars placed on the age estimate are  $\tau \pm \delta t$ , where  $\chi$  is twice as large at  $t = -(\tau \pm \delta t)$  than the minimum value at  $t = -\tau$ .

Figure 3 shows  $\Delta a_{p,j}$  for 70 Karin cluster members. To create this subset from the original list of 90 members, we

first eliminated 14 asteroids that have orbital uncertainties in semimajor axis larger than  $10^{-4}$  AU. Experimentation showed that the precision of our fit, as measured by  $\chi$ , degraded when orbital uncertainties larger than  $10^{-4}$  AU in  $a$  were considered.<sup>13</sup> We then eliminated six additional bodies for various reasons. Two of the six, 2001 SO88 and 2001 SH304, have incompatibly large differences between  $\Delta a_{p,j}^{\Omega}$  and  $\Delta a_{p,j}^{\varpi}$ ; this mismatch implies that they are probably interlopers. Four objects, (55434) 2001 TZ66, 2000 DU31, 2001 VU113, and 2002 AL107, are not shown in Fig. 3 for clarity. For some reason, these 4 objects have  $|\Delta a_{p,j}^{\Omega} - \Delta a_{p,j}^{\varpi}| = 2\text{--}3 \times 10^{-4}$  AU, values that are significantly larger than the ones determined for the remaining 70 objects. The remaining 70 members of the Karin cluster have  $|\Delta a_{p,j}^{\Omega} - \Delta a_{p,j}^{\varpi}| \lesssim 10^{-4}$  AU.

Our results for  $\tau = 5.7$  Myr and  $\tau = 5.8$  Myr are shown in Fig. 3 (panels (a) and (b), respectively). These two values of  $\tau$  bracket the age uncertainty and its effect on  $\Delta a_{p,j}$ . Both Figs. 3a and 3b display drift speeds of roughly the same magnitude. Several significant differences between the two sets, however, do exist. For example, panel (a) shows a marked asymmetry between the number of positive and negative  $\Delta a_{p,j}$ , with more negative than positive values. In contrast, panel (b) shows  $\Delta a_{p,j}$  with a more equal distribution. The largest object, (13807) 1998 XE13 ( $H = 13.7$ ), and most other Karin cluster members in panel (a) have larger negative drift speeds than in panel (b). Unfortunately, because our  $\tau$  value has some uncertainty, we cannot determine which of these results is correct. This is an important limitation of our study. To cope with this uncertainty, we discuss

<sup>13</sup> 55 out of the 70 selected orbits have better than  $10^{-5}$  AU orbital uncertainties in  $a$ . These uncertainties are required to achieve our target  $\sim 1^\circ$  alignment of  $\Omega_p$  and  $\varpi_p$  at  $t = -5.75$  Myr (see footnote 10).

both cases ( $\tau = 5.7$  and  $5.8$  Myr) whenever the differences between them become significant.

Despite these limitations, the results shown in Fig. 3 represent the first *direct* evidence that main-belt asteroids drift in the semimajor axis by non-gravitational effects. The measured magnitudes of the semimajor axis changes range from 0 to  $\sim 7 \times 10^{-4}$  AU.<sup>14</sup> We also find that  $\Delta a_P$  takes on larger values for objects with larger  $H$ , precisely as would be expected for semimajor axis drifts generated by size-dependent Yarkovsky thermal effects. In contrast, gravitational perturbations by (1) Ceres on  $a_P$  are size-independent (Vokrouhlický et al., 2001; Nesvorný et al., 2002b; Carruba et al., 2003). Before we compare the measured drift rates with theoretical predictions, however, we must first convert each Karin cluster member's  $H$  value into a diameter and then deal with the fact that we have limited information on their spin states and physical parameters.

#### 4. Comparison of determined drifts with models of the Yarkovsky effect

Little is known about the spin states and physical parameters of the Karin cluster members. Spectroscopic (R. Binzel, personal communication) and color observations (Jedicke et al., 2004; Nesvorný et al., 2004) suggest that the Karin cluster members are S-type asteroids (Bus and Binzel, 2002a, 2002b). S-type asteroids are rocky bodies that are believed to be composed predominately from Fe/Mg-bearing silicates such as olivine and pyroxene. This composition is consistent with the parent body of the Karin cluster being a member of the Koronis family (Binzel et al., 1993) and therefore physically comparable to (243) Ida, a Koronis family asteroid visited by the Galileo spacecraft (Belton et al., 1994). The taxonomic classification of the Karin cluster is important because it helps us to choose the appropriate albedo  $A$  needed to convert  $H$  into diameter  $D$ .

The mean albedo of main belt S-type asteroids determined using IRAS measurements is  $\approx 0.16$  (Tedesco et al., 2002). The mean albedo of Koronis family members from this same database is  $\approx 0.21$  (R. Jedicke, personal communication), a value consistent with Galileo observations of (243) Ida (Belton et al., 1994). These values, however, are better suited for larger main-belt asteroids than those found in the Karin cluster, particularly when one considers the possibility that asteroid albedos may be size-dependent (e.g., Binzel et al., 2002).<sup>15</sup> To deal with this issue, we will assume two values for albedo:  $A = 0.15$  which may be more appropriate for large Karin cluster members and  $A = 0.25$ , which

may be more appropriate for smaller bodies. We chose these values to show how results vary with  $A$ . Future direct determinations of  $A$  for Karin cluster members using infrared observations will help remove this uncertainty.

The spin periods ( $P$ ) of seven Karin cluster members are known (Yoshida et al., 2004); (13765) Nansmith, (28271) 1999 CK16, and 1998 SQ81 have spin periods  $P$  between 4.0 and 11 hr, (832) Karin and 1999 XE68 have  $P \approx 20$  hr, and (7719) 1997 GT36 and (43032) 1999 VR26 have  $P \approx 30$  hr. The first three  $P$  values are common among main-belt asteroids (Pravec et al., 2002) while the last four are long and perhaps atypical. These long periods cannot be attributed to thermal spin-down forces (e.g., the YORP effect; Rubincam, 2000; Vokrouhlický and Čapek, 2002; Vokrouhlický et al., 2003) because spinning-down an asteroid as large as (832) Karin ( $D \approx 20$  km) requires a timescale much longer than the Karin cluster's age. One possible explanation for these large  $P$  values is a combined scenario where (i) the parent body of the Karin was initially a slow rotator (possibly spun down by the YORP effect over the age of the Koronis family,  $\approx 2.5$  Gyr, Bottke et al., 2001), and (ii) little angular momentum was transferred from the impacting body into the largest fragment's rotation during the Karin cluster formation event. Results from numerical hydrocode impact experiments, where projectiles were shot into initially non-rotating target bodies, suggest that some barely-catastrophic collisions transfer little rotational angular momentum to the largest remnant (Love and Ahrens, 1997). A second possibility is that the catastrophic disruption event that produced the Karin cluster resulted in a net loss of rotational angular momentum for the largest remnant (e.g., Dobrovolskis and Burns, 1984). Further testing of these scenarios via numerical hydrocodes should provide interesting results.

The orbital results described here are linked to the orbit of (832) Karin, the central member and largest remnant of the Karin cluster. Karin, however, has undergone dynamical evolution over the last 5.75 Myr. To determine whether Karin's evolution has consequences for our results, we investigated its orbital history. If we assume (832) Karin has spin obliquity  $\epsilon = 45^\circ$ ,  $D \sim 20$  km, and  $P = 18.3$  hr, its predicted semimajor axis drift over 5.75 Myr via the diurnal Yarkovsky effect is  $\approx 3.7 \times 10^{-5}$  AU (using model of Vokrouhlický (1999) and our standard physical parameters described later). This value, which is comparable to the precision of our  $\Delta a_{P,j}$  measurements, is much smaller than the values of  $\Delta a_{P,j}$  determined for 1–6-km-diameter Karin cluster members (Fig. 3). Hence, for our purposes, we can safely neglect the semimajor axis drift of Karin itself. This effectively means that  $\delta a_{P,j} = \Delta a_{P,j}$  in the notation of Eqs. (3) and (4). Lightcurve observations capable of determining Karin's actual  $\epsilon$  value would help further refine these estimates.

At present, our limited knowledge about the physical properties of individual Karin cluster asteroids (e.g., their rotation periods, albedos, bulk and surface densities, surface

<sup>14</sup> These magnitudes are much larger than any of the uncertainties or of the neglected gravitational effects described above. For example, the orbital uncertainty in  $a_P$  is generally  $\lesssim 10^{-5}$  AU.

<sup>15</sup> Observations of near-Earth asteroids show that smaller asteroids have larger variations and generally larger albedo values than large asteroids. See, for example, Table 2 in Binzel et al. (2002).

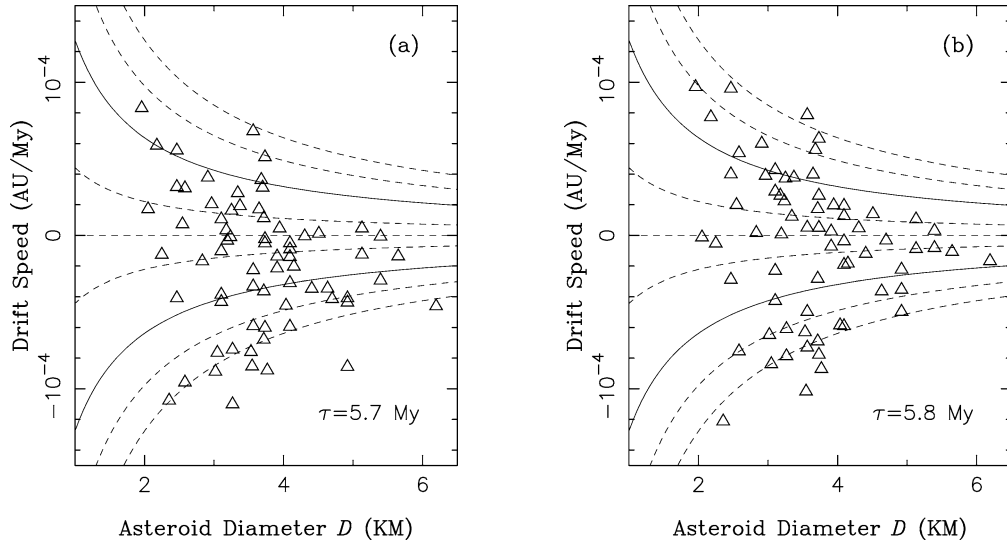


Fig. 4. Comparison between semimajor axis drift speeds predicted by our standard model with the ones determined for seventy Karin cluster members: (a)  $\tau = 5.7$  Myr, and (b)  $\tau = 5.8$  Myr. The lines show theoretical speeds of the semimajor axis drift for different asteroid obliquities  $\epsilon$ . From top to bottom,  $\epsilon = 0^\circ, 40^\circ, 60^\circ, 80^\circ, 90^\circ, 100^\circ, 120^\circ, 140^\circ, 180^\circ$ . The solid lines correspond to  $\epsilon = 60^\circ$  and  $120^\circ$ ; other lines are dashed. The symbols show semimajor axis drifts obtained for individual Karin cluster members from observations. We assumed albedo  $A = 0.15$ .

conductivities, spin obliquities, etc.) prevents us from precisely comparing their drift speeds with predictions based on Yarkovsky modeling (Vokrouhlický, 1998a, 1999). To circumvent this problem, we selected plausible physical parameters for all the bodies in our  $\approx 70$ -orbit data set and then made *statistical* comparisons between our model results and observations. Our goal is to determine whether the Yarkovsky effect, as described in the literature, is capable of explaining the observed drift rates on their own.

In our method, we use the linear model of the Yarkovsky effect for spherical bodies described by Vokrouhlický (1998a, 1999). In the following paragraph, we briefly describe this model and its dependence on various parameters. The effects of non-sphericity will be discussed later. See Vokrouhlický (1998a, 1998b, 1999) and Bottke et al. (2002) and the references therein for a more complete review of the subject.

The Yarkovsky force can be split into the so-called diurnal and seasonal components. The diurnal component is the radiation recoil force from the afternoon hemisphere of a rotating body. The seasonal component is produced by seasonal heating and cooling of a body's surface as it orbits the Sun. Objects having zero or infinitely fast rotation rates experience no diurnal Yarkovsky effect. A multi-km asteroid is subject to a diurnal Yarkovsky force proportional to  $\cos \epsilon$ . Unlike the diurnal effect, the seasonal Yarkovsky effect is independent of the sense of rotation of a body. It scales with obliquity as  $\sin^2 \epsilon$  and produces a decay in the body's semimajor axis. The timescale for semimajor axis decay via the seasonal effect is generally longer than that for changes of  $a_P$  via the diurnal effect (unless  $\epsilon \sim 90^\circ$ ). For large objects (such as the multi-km members of the Karin cluster), the Yarkovsky force scales as  $1/D$ . Surface conductivity  $K$  is another important parameter that influences the strength of the Yarkovsky effect. Values for  $K$  range from

$\approx 0.001 \text{ W m}^{-1} \text{ K}^{-1}$  for highly-porous or regolith-covered surfaces to  $\approx 1 \text{ W m}^{-1} \text{ K}^{-1}$  for bare rock or icy objects to  $\approx 40 \text{ W m}^{-1} \text{ K}^{-1}$  for iron objects.

We inserted Eqs. (4) and (5) of Bottke et al. (2002) into a computer code which, depending on the physical parameters and spin state of our asteroids, calculates orbital drift in  $a_P$ . To compare the measured drift speeds (Fig. 3) with those predicted by our Yarkovsky model, we adopt the following parameters: (i) surface thermal conductivity  $K = 0.005 \text{ W m}^{-1} \text{ K}^{-1}$  (corresponding to a regolith-covered surface), (ii) bulk asteroid density  $\rho = 2.5 \text{ g cm}^{-3}$  (a value believed to be common among km-sized S-type asteroids, Hilton, 2002; Britt et al., 2002), (iii) surface density  $\rho_s = 1.5 \text{ g cm}^{-3}$  (corresponding to asteroids with regolith on their surface), and (iv) rotation period  $P = 5$  hr. We will also assume albedos  $A = 0.15$ , characteristic for large S-type asteroids, and  $A = 0.25$ , possibly the relevant value for km-sized Karin cluster members.

By experimenting with our code, we found the maximum drift speeds produced by the seasonal effect account for, at most, 10% of the drift speeds generated by the diurnal effect for  $\epsilon = 45^\circ$ . This result is robust over a large range of physical parameters and spin periods. For this reason, the seasonal effect is neglected in our results described below. Note that the exclusion of the seasonal effect means our predicted drift speeds will be symmetric with respect to  $\epsilon$ .

Figures 4 ( $A = 0.15$ , model I) and 5 ( $A = 0.25$ , model II) compare the semimajor axis drift speeds predicted by our model with those determined for the 70 Karin cluster members described in Section 3 (we take the arithmetic mean of the two measurements of  $\Delta a_P$  from  $\Omega_P$  and  $\varpi_P$  shown in Fig. 3, and list these values in Table 2). This comparison shows an exciting result: the measured drift speeds  $\dot{a}_P$  are nearly identical to those predicted by our standard

Table 2

Drift speeds and obliquities of the Karin cluster members determined in two models: (I)  $A = 0.15$  and  $\tau = 5.8$  Myr (columns 3–5) and (II)  $A = 0.25$  and  $\tau = 5.7$  Myr (columns 6–8)

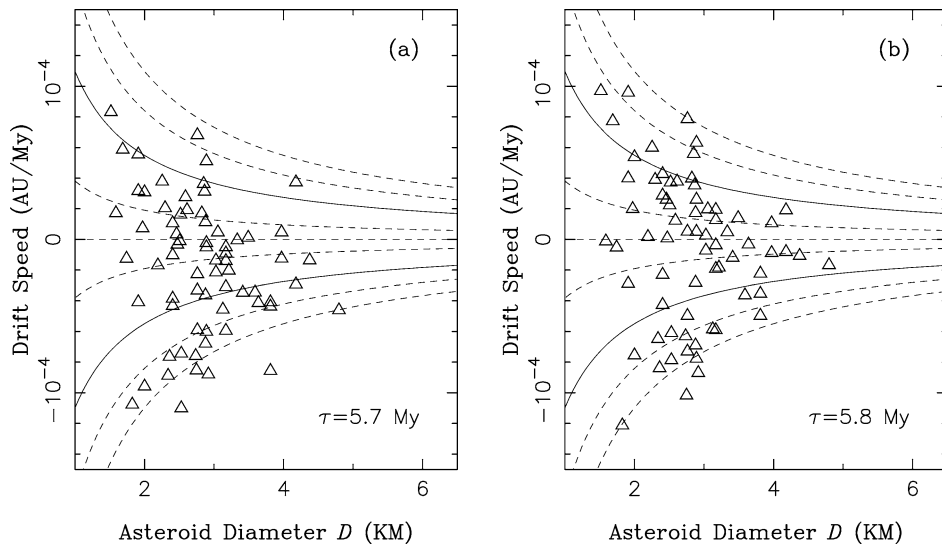
Number	Name	$A = 0.15, \tau = 5.8$ Myr			$A = 0.25, \tau = 5.7$ Myr		
		$D$ (KM)	$10^5 \times \dot{a}$ (AU Myr $^{-1}$ )	$\epsilon$ (deg)	$D$ (KM)	$10^5 \times \dot{a}$ (AU Myr $^{-1}$ )	$\epsilon$ (deg)
832	Karin	20.1	–	–	15.6	–	–
7719	1997 GT36	5.5	–0.77	99	4.3	–3.0	125
10783	1991 RB9	5.7	–1.1	104	4.5	–1.4	106
11728	Einer	5.0	–3.5	133	3.9	–4.4	141
13765	Nansmith	5.0	–4.9	164	3.9	–8.6	~ 180
13807	1998 XE13	6.3	–1.6	113	4.9	–4.7	~ 180
15649	6317 P-L	4.2	–5.9	164	3.2	–5.9	151
16706	Svojsik	3.6	–7.3	~ 180	2.8	–5.9	139
20089	1994 PA14	3.6	–5.0	135	2.8	–3.3	115
20095	1994 PG35	5.0	–2.1	115	3.9	–4.1	137
23054	1999 XE42	3.1	4.3	58	2.4	1.0	83
23338	2809 P-L	3.3	3.8	61	2.6	1.6	79
26970	1997 SE2	3.0	3.9	62	2.3	2.0	78
28271	1999 CK16	4.8	–0.25	93	3.7	–4.2	135
33143	1998 DJ7	4.2	2.0	71	3.2	–0.53	94
34312	2000 QO188	3.6	0.57	85	2.8	–2.3	107
40510	1999 RU87	4.2	1.3	77	3.2	–1.4	102
40782	1999 TX26	4.0	0.30	87	3.1	–1.4	101
40789	1999 TW31	3.8	–7.8	~ 180	2.9	–6.0	143
40921	1999 TR171	3.8	2.7	67	2.9	–0.27	92
41307	1999 XA149	2.5	–2.9	106	1.9	–4.1	111
43032	1999 VR26	4.2	–1.9	108	3.2	–3.1	117
47640	2000 CA30	5.5	0.32	86	4.3	–0.07	91
48369	4153 T-2	3.8	6.3	19	2.9	5.1	47
50715	2000 EV136	3.8	0.53	85	2.9	–0.52	94
51068	2000 GW156	3.2	–4.3	122	2.4	–3.8	115
51089	2000 GO178	3.2	3.0	69	2.4	–1.1	97
51923	2001 QD95	2.6	–7.5	141	2.0	–9.6	153
52009	2002 EU146	2.4	–12	~ 180	1.9	–11	155
55124	2001 QU170	2.9	0.21	89	2.2	–1.7	100
55852	1996 TS34	2.1	–0.15	91	1.6	1.8	83
56285	1999 LJ3	2.3	–0.50	93	1.8	–1.3	96
57735	2001 UQ159	3.6	7.9	~ 0	2.8	6.8	30
	1994 EX	4.6	1.4	75	3.6	0.11	89
	1995 EC5	3.1	–6.4	141	2.4	–8.9	165
	1995 TH10	3.4	3.8	59	2.7	1.9	77
	1995 UN13	4.0	–0.69	96	3.1	–2.2	108
	1998 SQ81	5.2	–0.87	100	4.0	–1.2	103
	1999 TV145	4.1	–5.9	161	3.2	–4.5	131
	1999 VM71	3.3	–6.1	142	2.6	–7.5	151
	1999 VW121	2.5	9.7	18	1.9	5.5	61
	1999 VV155	2.6	2.0	78	2.0	0.72	86
	1999 XD38	3.4	1.2	81	2.6	2.8	70
	1999 XE68	4.4	0.49	85	3.4	–0.06	90
	2000 DH36	3.3	2.3	73	2.6	–0.14	91
	2000 HN72	4.2	–1.8	107	3.27	–2.0	107
	2000 QQ18	3.7	4.0	54	2.87	1.7	77
	2000 QM81	3.8	3.5	59	2.91	3.1	65
	2000 SX40	2.6	5.4	56	2.03	3.1	74
	2000 SR228	2.0	9.7	41	1.54	8.3	54
	2000 UV4	3.8	–8.7	~ 180	2.97	–8.8	~ 180
	2000 UE79	3.7	5.6	34	2.9	3.6	62
	2000 VE21	3.0	6.1	45	2.29	3.8	67
	2000 YQ59	5.2	1.1	77	4.04	0.46	85
	2001 QF18	4.5	–1.1	102	3.47	–3.5	123
	2001 QP94	3.6	–10	~ 180	2.79	–8.5	~ 180
	2001 SH169	3.2	2.7	70	2.5	0.31	88
	2001 TW49	3.8	–6.9	~ 180	2.92	–6.8	154

(continued on next page)

Table 2 (continued)

Number	Name	$A = 0.15, \tau = 5.8 \text{ Myr}$			$A = 0.25, \tau = 5.7 \text{ Myr}$		
		$D$ (KM)	$10^5 \times \dot{a}$ (AU Myr $^{-1}$ )	$\epsilon$ (deg)	$D$ (KM)	$10^5 \times \dot{a}$ (AU Myr $^{-1}$ )	$\epsilon$ (deg)
2001 UA133		2.2	7.8	48	1.71	5.8	63
2001 XU92		4.0	2.0	72	3.1	0.45	86
2001 XD232		3.3	-7.8	$\sim 180$	2.57	-11	$\sim 180$
2002 AO172		3.6	-6.3	152	2.78	-7.6	164
2002 CV38		2.5	4.0	67	1.94	3.2	74
2002 CL81		3.1	-8.4	$\sim 180$	2.4	-7.6	146
2002 CX104		3.8	-2.8	114	2.92	-3.7	119
2002 CV120		3.2	-2.3	106	2.44	-4.4	119
2002 SQ20		3.2	0.08	89	2.51	-0.34	92
2002 TJ250		4.2	-0.36	93	3.22	-0.92	98
2002 TO257		3.8	1.8	75	2.92	1.1	81
2247 T-2		4.7	-3.6	132	3.65	-3.4	125

The columns are: number and name of an asteroid, its diameter ( $D$ ) assuming  $A = 0.15$ , drift speed in  $a_P$  ( $\dot{a}_P$ ) assuming  $\tau = 5.8$  Myr, estimated obliquity in model I ( $\epsilon$ ), diameter ( $D$ ) assuming  $A = 0.25$ , drift speed in  $a_P$  ( $\dot{a}_P$ ) assuming  $\tau = 5.7$  Myr, estimated obliquity in model II ( $\epsilon$ ). Both models assume  $K = 0.005 \text{ W m}^{-1} \text{ K}^{-1}$ . The values of  $\epsilon$  vary within  $\pm 15^\circ$  around the listed values if  $K$  is varied within  $0.05\text{--}0.0001 \text{ W m}^{-1} \text{ K}^{-1}$ .


 Fig. 5. The same as Fig. 4 but with  $A = 0.25$ .

model of the Yarkovsky effect! This result was not expected a priori. In fact, the measured drift speeds (of unknown origin) could easily have been orders of magnitude lower or higher than our model values. The fact they are comparable strongly implies that the detected drift speeds were produced predominately by the Yarkovsky effect. Thus, these results provide the first direct measurement of how the Yarkovsky effect modifies the semimajor axes of real main-belt asteroids. It also validates the global theoretical framework of Yarkovsky evolution developed over the last several years (e.g., Farinella and Vokrouhlický, 1999; Bottke et al., 2002; Morbidelli and Vokrouhlický, 2003).

We now compare our measurements to predictions based on Yarkovsky modeling in greater detail. Because we do not know the obliquities of individual bodies, we cannot precisely compare our individual measurements with the  $\dot{a}_P$  values found in Figs. 4 and 5. Instead, we compare our max-

imum and mean  $|\dot{a}_P|$  for an ensemble of bodies with those predicted for asteroids evolving with  $\epsilon = 0^\circ$  and  $\epsilon = 60^\circ$ , respectively. If the spin axes of Karin cluster members have random orientations (such a spin axis distribution might be expected for fragments produced by a collisional disruption event),  $\cos \epsilon$  should have a uniformly random distribution, which in turn should set the magnitudes of the maximum and mean drift speeds of the ensemble equal to drift speeds for  $\epsilon = 0^\circ$  (or  $180^\circ$ ) and  $\epsilon = 60^\circ$ , respectively (Bottke et al., 2002).

Several bodies in Figs. 4 and 5 have measured  $|\dot{a}_P|$  values that are somewhat larger than the maximum drift speeds predicted by our Yarkovsky model. This discrepancy is best visible in Fig. 4a, where 8 bodies with negative drift speeds (including the second largest Karin cluster member, (13807) 1998 XE13) show  $|\dot{a}_P|$  that are 10–50% larger than the maximum theoretical drift speed for  $\epsilon = 180^\circ$ . It is possible

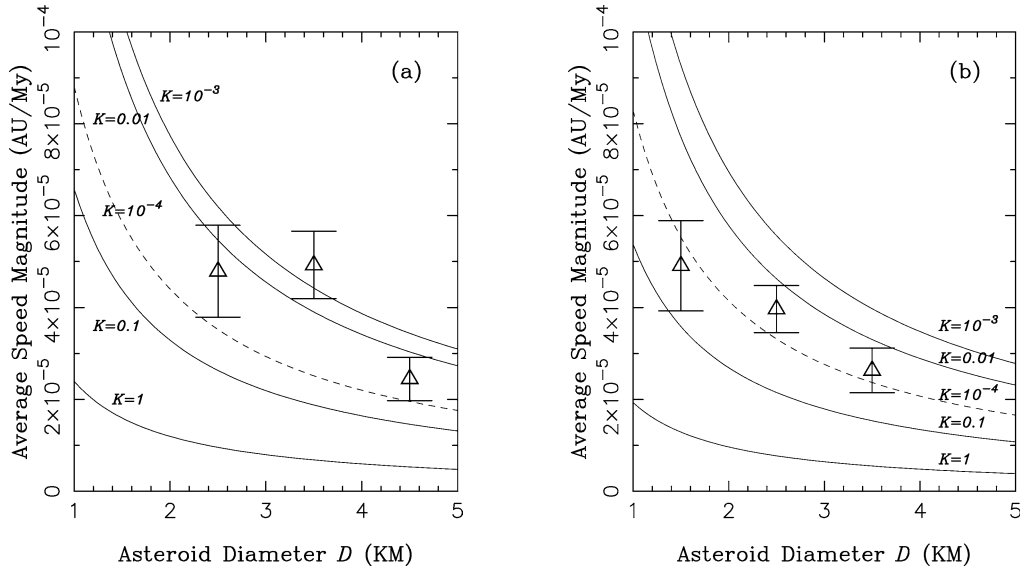


Fig. 6. Comparison of mean drift speeds with  $\dot{a}_p$  predicted theoretically: (a)  $A = 0.15$  and  $\tau = 5.8$  Myr, and (b)  $A = 0.25$  and  $\tau = 5.7$  Myr. The symbols and error bars show the mean data that we have obtained by averaging  $|\dot{a}_p|$  over bodies within a 1-km diameter range around  $D$ , where our statistics was good (we required more than ten bodies in a diameter bin). The lines show theoretical drift speeds for  $\epsilon = 60^\circ$  and several values of surface thermal conductivity  $K$ . From top to bottom, the solid lines show results for  $K = 10^{-3}$ , 0.01, 0.1, and  $1 \text{ W m}^{-1} \text{ K}^{-1}$ . The dashed line corresponds to  $K = 10^{-4} \text{ W m}^{-1} \text{ K}^{-1}$ .

that we are detecting a real physical effect here. For example, these bodies may have experienced a close encounter with (1) Ceres in the past that altered their  $a_p$  values (Section 5). Alternatively, these asteroids may have  $\epsilon \sim 0$  and large  $A$ . Indeed, Fig. 5, generated using  $A = 0.25$ , shows fewer outliers than Fig. 4, generated using  $A = 0.15$ . We also note that  $\tau = 5.8$  Myr (Figs. 4 and 5) produces smaller  $|\dot{a}_p|$  that are generally more compatible with maximum predicted  $|\dot{a}_p|$ . The drift speeds  $\dot{a}_p$  are listed in Table 2 for  $\tau = 5.8$  Myr and  $A = 0.15$  (left columns) and for  $\tau = 5.7$  Myr and  $A = 0.25$  (right columns).

To compare our drift speeds, we binned the measured drifts according to an object's diameter  $D$ , we took the arithmetic mean for each  $D$ , and computed the theoretical  $\dot{a}_p$  value using  $D$ ,  $\epsilon = 60^\circ$  and several values of surface thermal conductivity  $K$  (Fig. 6). We infer from Fig. 6 that our results are incompatible with  $K > 0.1 \text{ W m}^{-1} \text{ K}^{-1}$  because the determined  $\langle \dot{a}_p \rangle$  values determined for these values of  $K$  are significantly larger than the predicted  $\dot{a}_p$  values for  $\epsilon = 60^\circ$ . This result suggests that asteroid surfaces within the Karin cluster are not bare rock (nor any other moderately to highly-conductive material). Instead, our data suggests these  $\approx 5.75$ -Myr old asteroid fragments are covered by some low-conductive material such as the fine-grained regolith. This low-conductive regolith layer may be thin because the penetration depth of the diurnal thermal wave is  $\lesssim 5$  cm (e.g., Vokrouhlický, 1998a). The origin of this putative regolith is unknown. It could have been deposited in the aftermath of the breakup event, when dust grains settled on the surfaces of larger fragments, or it could have been gradually produced over the past  $\approx 5.75$  Myr by impacts. To any event, km-sized and larger Karin cluster members most likely have had at least some regolith on their surfaces over

the last 5.75 Myr. This conclusion is consistent with those of Chesley et al. (2003), who showed by radar ranging that 0.5 km near-Earth Asteroid (6489) Golevka may also have a regolith-covered surface.

Plausible values of  $K$  for Karin cluster members range between 0.1 to  $10^{-4} \text{ W m}^{-1} \text{ K}^{-1}$ . We cannot yet constrain  $K$  more precisely because the data in Fig. 6 show a large scatter for different  $D$ . A different way to explain this scatter, however, would be to assume that Karin cluster members do not have randomly-oriented spin axes.

To investigate this issue, we assumed that the drift speeds predicted by our standard Yarkovsky model (i.e.,  $K = 0.005 \text{ W m}^{-1} \text{ K}^{-1}$ ) were equivalent to our measured values. This approximation allows us to solve for  $\epsilon$  for every asteroid in our sample. Table 2 lists these  $\epsilon$ , while Fig. 7 shows the same data as a histogram. We caution that these values should not be taken too seriously because our assumptions have introduced large uncertainties into our solutions. For example, as we will show in the next section, gravitational perturbations from (1) Ceres may account for changes of up to  $\sim 10^{-4}$  AU in  $a_p$  over 5.75 Myr, which is  $\lesssim 30\%$  of the average drift speeds shown in Fig. 6. Moreover, the function  $\epsilon \propto \arccos(\dot{a}_p)$  is degenerate for  $\epsilon \sim 90^\circ$ , which indicates the values of  $\epsilon$  close to  $90^\circ$  are not well constrained by measured  $\dot{a}_p \sim 0$ .

The results from Fig. 7 suggest the spin axes orientations of Karin cluster members are essentially random. Peaks and dips in the distribution are mainly due to our small-number statistics. Only the largest Karin cluster members show significant deviations from a uniformly random distribution of  $\cos \epsilon$  ( $D > 4$  km in (a) and  $D > 3$  km in (b)). If we can trust these results, the largest Karin cluster members are preferentially retrograde rotators. Though this result needs to be

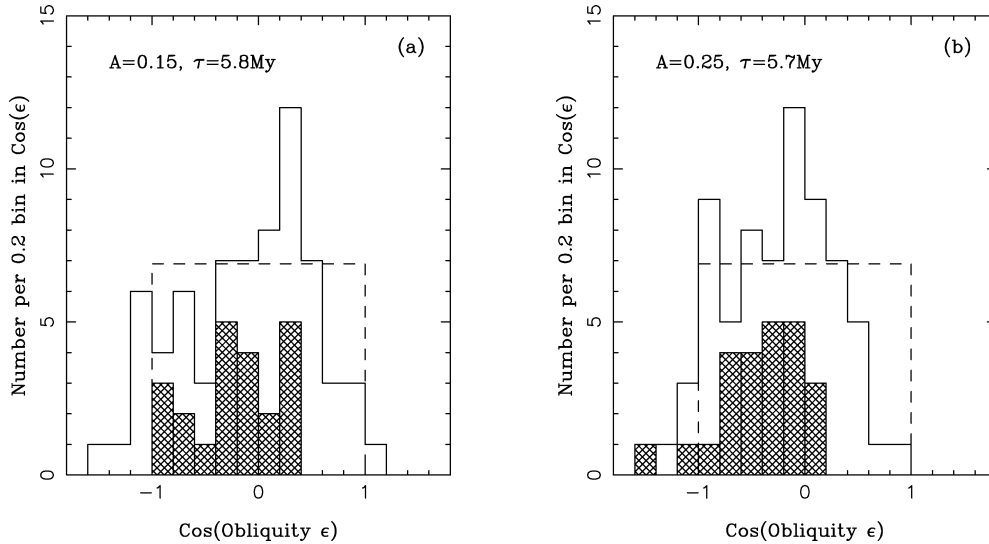


Fig. 7. Histogram of obliquities  $\epsilon$  determined in model I (panel (a),  $A = 0.15$ ,  $\tau = 5.8$  Myr) and in model II (panel (b),  $A = 0.25$ ,  $\tau = 5.7$  Myr). The solid lines show distributions of  $\cos \epsilon$  for seventy Karin cluster members. The dashed lines were plotted for a reference. They show uniformly random distributions in  $\cos \epsilon$ . Hatched histograms show distributions of  $\cos(\epsilon)$  for large members:  $D \geq 4$  km (a) and  $D \geq 3$  km (b). We found that a majority of large members of the Karin cluster are retrograde rotators. Values on  $X$  axis that are either  $> 1$  or  $< -1$  refer to objects for which we did not find a plausible value of  $\epsilon$  with assumed parameters. These objects probably have  $\epsilon \sim 0^\circ$  or  $\epsilon \sim 180^\circ$ , respectively (Table 2).

confirmed observationally, it might suggest that the largest Karin cluster member somehow ‘remember’ the geometry of the  $t \approx -5.75$  Myr impact event.

We were unable to find a plausible  $\epsilon$  value for several Karin cluster members because their measured drift speeds were too fast to be matched by the parameters of our standard model. These asteroids are listed in Table 2 as having  $\epsilon \sim 0$  or  $\epsilon \sim 180^\circ$ . No simple explanation for this problem exists. For example, choosing a different  $K$  value for these objects (rather than  $K = 0.005 \text{ W m}^{-1} \text{ K}^{-1}$ ) does not remedy the problem because no plausible  $K$  value is capable of reproduce their  $\dot{a}_P$  values. Similarly, no plausible  $P$  values can produce the determined  $\dot{a}_P$  values. We speculate that some combination of the following factors may play some role here. These asteroids may have: (i) faster drift speeds than predicted by theoretical models, (ii) high albedos ( $\gtrsim 0.3$ ), (iii) densities  $\lesssim 2 \text{ g cm}^{-3}$ , and/or (iv) their  $a_P$  changed as a result of encounters to (1) Ceres. We discuss this last possibility in the next section.

## 5. Effect of (1) Ceres

We have argued in previous sections that the semimajor axis drifts of Karin cluster members are comparable with those expected from the Yarkovsky effect. An issue we have not yet discussed is whether close encounters with (1) Ceres (and, to a lesser degree, other large main-belt asteroids) are capable of significantly modifying their  $a_P$  values as well. Nesvorný et al. (2002b, see also Carruba et al., 2003) showed that (1) Ceres predominantly produces small and subtle changes to  $a_P$  values among main-belt asteroids. We cannot rule out the possibility a priori, however, that

a few Karin cluster members have experienced meaningful changes to their orbits via close encounters with Ceres.

To investigate this problem, we numerically integrated the orbits of 70 Karin cluster members in a simulation where Ceres’ gravitational perturbations were explicitly included. The Karin cluster members were treated as massless test particles in the experiment. Their orbits were identical to the ones used in Section 2. The mass of Ceres was set to  $4.7 \times 10^{-10} M_\odot$ , where  $M_\odot$  is the mass of the Sun (Michalak, 2000). Perturbations by other asteroids were ignored because Nesvorný et al. (2002b) and Carruba et al. (2003) concluded their perturbations are much smaller than those provided by Ceres. As a control, we also numerically integrated the same test bodies without Ceres. Both runs included the planets Venus–Neptune; their orbits and masses are described in Section 2. We used a 5-day time step for our integrations and we tracked the bodies for 10 Myr using an  $N$ -body integrator known as SyMBA (Duncan et al., 1998; Levison and Duncan, 2000). SyMBA has the speed of highly efficient integration algorithms using Wisdom–Holman mapping (Wisdom and Holman, 1991), but it can also accurately handle close encounters between bodies by employing a variant of multiple step-size techniques (Biesiadecki and Szeel, 1993).

We found that orbital changes of Karin cluster members due to encounters with Ceres are, for the most part, significantly smaller than those shown in Fig. 3. For example, the  $1\text{-}\sigma$  variation of  $a_P$  over 5.75 Myr is  $\approx 10^{-4}$  AU, a value that is only a small fraction of the observed spread of  $\Delta a_P$  (Fig. 3). Although to first order this validates our assumption from the previous section that the effect of Ceres can be neglected in order to understand the evolution of an ensemble of objects, our results indicate that its effects

cannot be ignored completely. Indeed, perturbations from Ceres introduce additional uncertainties into our comparison of observed  $\Delta a_p$  with those predicted by the Yarkovsky effect, because it may account for some portion of this value ( $\approx 10^{-4}$  AU). These uncertainties are larger than those originating from our imperfect knowledge of Karin cluster member orbits, their initial  $\delta V$ , or the precision of our proper elements because  $\Delta a_p \approx 10^{-4}$  AU may produce up to  $\sim 5^\circ$  uncertainties in  $\Delta \Omega_p$  and  $\Delta \varpi_p$  at  $t = -5.8$  Myr.

It is problematic to ‘remove this noise’ from our analysis in the previous sections because it is difficult (if not impossible due to chaos) to determine the  $\Delta a_p$  signature produced by Ceres for individual Karin cluster members. This problem is less relevant for sub-km Karin cluster members (and for small members of other recently-formed families) because the strength of the Yarkovsky effect increases with  $1/D$  while the effect of (1) Ceres is size-independent. In this sense, the sub-km main-belt asteroids have better signal-to-noise ratio to probe effects of the Yarkovsky force.

The effect of Ceres on  $\Delta a_p$  potentially explains why some of our analyzed orbits have larger drift speeds than those predicted by Yarkovsky models (listed as  $\epsilon \sim 0^\circ$  or  $\epsilon \sim 180^\circ$  in Table 2). This result also suggests one take extra caution in interpreting the values of  $\epsilon$  shown in Table 2 because the effect of Ceres was neglected in those estimates. On the other hand, the effect of Ceres cannot explain why large Karin cluster members are predominantly retrograde rotators because stochastic gravitational perturbations by Ceres produce equal number of positive and negative  $\Delta a_p$ .

The combined effects of Ceres and chaotic resonances (e.g., Nesvorný et al., 2002c) on  $e_p$  and  $i_p$  are less of a concern because their  $1\text{-}\sigma$  variations over 5.75 Myr are only  $5.3 \times 10^{-5}$  and  $1.7 \times 10^{-5}$  rad, respectively. These variations produce smaller than  $1^\circ$  uncertainties in  $\Delta \Omega_p$  and  $\Delta \varpi_p$  at  $t = -5.75$  Myr. Hence, they can be safely ignored.

## 6. Numerical integration with the Yarkovsky effect included

In Section 3, we estimated the semimajor axis drifts of Karin cluster members using a numerical integrator that did not include Yarkovsky thermal forces. In Section 4, we argued that the magnitude of these drifts can be best explained by the Yarkovsky effect. This motivated us to perform a new numerical simulation where the Yarkovsky effect was explicitly accounted for at each time step. These new runs are an improvement over those described in Section 3 because they allow our drifting Karin cluster members to interact with nearby tiny resonances (see Bottke et al., 2001 for a similar study).

We used a version of the Wisdom–Holman map (Wisdom and Holman, 1991) distributed in *Swift* code (Levison and Duncan, 1994) that was modified to account for the Yarkovsky force (Brož, 1999). Using this modified code,

we tracked orbits of the 70 Karin cluster members listed in Table 2. We included the gravitational perturbations of the planets Venus–Neptune. To calculate the Yarkovsky force for each individual asteroid, we used our standard physical parameters (described in Section 4) and Table 2 obliquity values for  $\tau = 5.8$  Myr.

To set up the initial orbits, we extracted the instantaneous orbits of the planets and asteroids at  $t = -5.8$  Myr from the numerical integration results described in Section 2. The  $a$  values obtained by this method were then shifted by the amounts listed in Table 2 in an attempt to mimic the original  $a$ . The other orbital elements were kept unchanged. We tracked these orbits into the future for 10 Myr using a 5-day time step. The proper elements of each individual orbit were calculated in 10,000-yr intervals using the methods described in Sections 2 and 3. Because these orbits were evolving via thermal effects, and to avoid spurious effects, we used a shorter interval  $\Delta t \approx 1$  Myr for the FMFT than those used in Sections 2 and 3. Using this  $\Delta t$  value, angles  $\Omega_p$  and  $\varpi_p$  have better than  $1^\circ$  precision for any  $t$ .

Figure 8 shows the putative past orbital histories of  $\Omega_p$  and  $\varpi_p$  for our 70 Karin cluster members. To make these angles at  $t = 0$  compatible with their current values, we adjusted them in the following way. For each individual object, we calculated the differences  $\delta \Omega$  and  $\delta \varpi$  at  $t = 0$  between the current values of  $\Omega_p$  and  $\varpi_p$  and the values obtained from this integration. The integrated values of  $\Omega_p$  and  $\varpi_p$  obtained at time  $t$  were then offset by  $\delta \Omega$  and  $\delta \varpi$ . With this

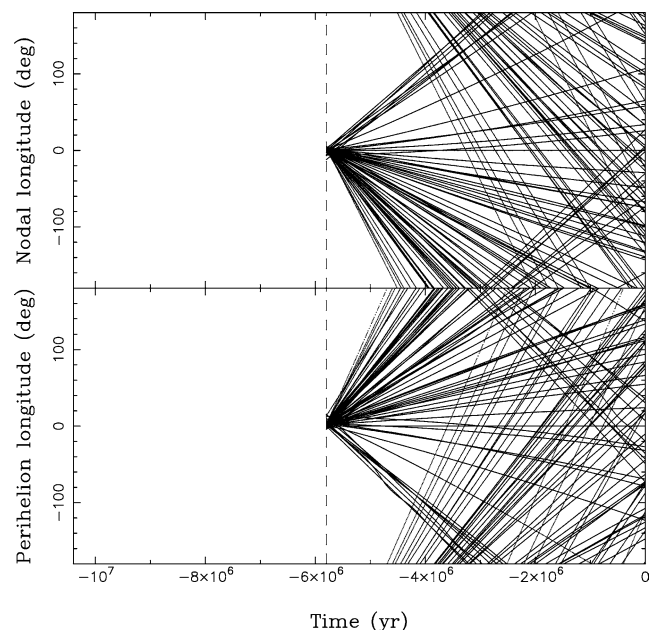


Fig. 8. The plot shows past orbital histories of seventy members of the Karin cluster: (top) proper nodal longitude  $\Omega_p$  and (bottom) proper perihelion longitude  $\varpi_p$ . Values of these angles relative to (832) Karin are shown. This figure is similar to Fig. 2. Here, however, we accounted for the Yarkovsky effect explicitly in the integration. As a result, the convergence of secular angles at  $t \approx -5.8$  Myr significantly improved. The total spreads of  $\Delta \Omega_p$  and  $\Delta \varpi_p$  at  $t = -5.8$  Myr are  $\pm 5^\circ$ , about an order of magnitude smaller than in Fig. 2, where the effects of the Yarkovsky force were ignored.

adjustment, the orbital elements converge *exactly* to their current values at  $t = 0$ .

Figure 8 can be compared to Fig. 2. As expected, the convergence of secular angles at  $t \approx -5.8$  Myr in Fig. 8 is significantly better because we accounted for the Yarkovsky effect explicitly in the integration. As a result, the total spread of  $\Delta\Omega_p$  and  $\Delta\varpi_p$  at  $t = -5.8$  Myr are  $\pm 5^\circ$ , about an order of magnitude smaller than in Fig. 2 where the effects of the Yarkovsky force were ignored. The mean values of  $\Delta\Omega_p$  and  $\Delta\varpi_p$  calculated over the 70 integrated orbits at  $t = -5.8$  Myr are only  $2^\circ$  and  $2.5^\circ$ , respectively.

This result represents an important validation of our previous conclusions where we argued that the past orbital histories of Karin cluster members need to be corrected for the Yarkovsky effect. It also shows that the linear model of the Yarkovsky effect combined with our chosen physical parameters and Table 2 obliquities represents a plausible (if potentially non-unique) solution to the problem motivated by the poor alignment of the orbits at  $t = -5.8$  Myr in Fig. 2.

Because we did not detect any substantial irregularities in the orbital evolution of test bodies drifting through tiny resonances located near the Karin cluster, the semimajor axis drift speeds of Karin cluster members may be, in principle, adjusted by slightly changing their  $\epsilon$  values to further reduce  $\Delta\Omega$  and  $\Delta\omega$  at  $t = -5.8$  Myr. This process may be iterated until  $\Delta\Omega_j \lesssim 1^\circ$  and  $\Delta\omega_j \lesssim 1^\circ$  for most  $j$ . In practice, however, the effects of (1) Ceres and other uncertainties of our model may prohibit such a convergence. We believe that additional observational data needs to be collected before such an advanced theoretical study can be successfully attempted.

## 7. Discussion and conclusions

Here we briefly summarize the main results of this study:

- (1) Using numerical techniques, we have produced the largest data set of Karin cluster members that can be extracted from current observations (90 objects; Table 1). This list does not include the previously-believed second largest member of the Karin cluster, (4507) 1990 FV. Our work in this paper suggests this object is an interloper. Consequently, the estimated size of the parent body of the Karin cluster, assuming all the fragments have an albedo of  $A = 0.21$ , is now  $D \sim 20$  km, somewhat lower than the one given by Nesvorný et al. (2002a). We caution, however, that because we have yet to identify many  $D < 10$  km Karin cluster members, this value should be considered a lower limit.<sup>16</sup> This conclusion also changes the size-distribution con-

straints used by Michel et al. (2003) for SPH impact experiments. Our work identified many  $D = 1\text{--}3$  km Karin cluster members. Small Karin cluster members represent an important constraint on the size-frequency and the ejection-velocity distributions of the fragments created by catastrophic disruptions. We confirmed and slightly revised the age of the Karin cluster by numerically tracking the orbits of 70 member asteroids into the past. Our best estimate of the age of the Karin cluster is now 5.75 Myr with the nominal error of  $\sim 0.05$  Myr (see Section 3 for the definition of our nominal error).

- (2) We have measured, for the first time, the speed that main-belt asteroids evolve in the semimajor axis due to the non-gravitational effects. The magnitude of these measured speeds is similar to those predicted by theoretical models of the Yarkovsky force (Vokrouhlický, 1999). Taken together, our results represent the first direct detection of the Yarkovsky effect for main-belt asteroids, and they validate in significant ways the asteroid thermal models described in the recent literature (e.g., Vokrouhlický, 1999). Our work is complementary to the first direct (radar) detection of the Yarkovsky effect on a near-Earth asteroid (Chesley et al., 2003), except here our method allowed us to examine a large sample of multi-km main-belt asteroids with different obliquities, spin periods, etc. Both radar and our methods have a promising future. The expectations are to obtain one or two new radar detections each year in the next decade (Vokrouhlický et al., 2004). Based on the current rate of continuing discoveries of main-belt asteroids and calculations of family assignments, we expect to detect the Yarkovsky effect for  $\sim 35$  new Karin family members by 2006.
- (3) Measured drift speeds for several Karin cluster members are 10–50% larger than the maximum drift speeds predicted by the theory of the Yarkovsky effect. For example, Asteroids 2000 UV4, 2001 QP94 and 2001 XD232 all have large negative  $\dot{a}_p$  values. Other examples are listed in Table 2. These asteroids may have (i)  $\epsilon \sim 0^\circ$  or  $180^\circ$ , (ii) faster drift speeds than predicted by theoretical models that assume the asteroids have spherical shapes (the Yarkovsky effect may be somewhat larger or smaller for realistic asteroidal shapes; Vokrouhlický, 1998b), (iii) higher albedos ( $\gtrsim 0.3$ ) than assumed by our model, (iv) densities  $\lesssim 2$  g cm<sup>-3</sup>, and/or (v) their  $a_p$  values were modified by close encounters with (1) Ceres. We believe these objects may be interesting observational targets because some of our above speculations are testable by lightcurve and infrared observations.
- (4) By extrapolating the measured semimajor axis drift rates in time, we estimate that the Karin cluster would disperse in  $\sim 100$  Myr to a degree where HCM cannot separate it from the background population of asteroids. Because about four Karin-like families exist in the main belt today (Nesvorný et al., 2003) we found that one 20–30-km-sized asteroid is catastrophically dis-

<sup>16</sup> Short time before submission of this paper (on 10-Feb-2004) we searched for additional Karin cluster members using latest asteroid orbital element catalog. We found five new candidates: 2003 QK39, 2003 UR136, 2003 HH6, 2003 BH89, 2003 SJ214. These asteroids have absolute magnitudes that range between 14.6 and 16.4 suggesting  $D = 1\text{--}4$  km.

rupted in the main belt every 25 Myr. This implies a surprisingly low rate of disruptions that may be consistent with an increasing appreciation that asteroids are more difficult to disrupt by impacts than believed previously (Cheng and Barnouin-Jha, 1999; Chapman et al., 1999; Benz and Asphaug, 1999).

- (5) Our results suggest that the 1–6-km diameter Karin cluster members have surface conductivities  $K < 0.1 \text{ W m}^{-1} \text{ K}^{-1}$ , consistent with them having surface regolith. It is important to note that because we measure *average* drift speeds over the past  $\approx 5.75$  Myr, we do not know whether this regolith was deposited in immediate aftermath of the Karin cluster formation event or whether it was produced over time by impacts. What we can say is that the evolution histories of the cluster members are consistent with the presence of surface regolith over most/all of their 5.75 Myr lifetimes. This low-conductive regolith layer may be thin because the penetration depth of the diurnal thermal wave is  $\lesssim 5$  cm (e.g., Vokrouhlický, 1998a).
- (6) Table 2 lists tentative values of obliquities  $\epsilon$  for 70 small main-belt asteroids. This unique data set may be used to study spin states of asteroid fragments generated by erosional collisions, particularly because multi-km Karin cluster member are too young to have undergone substantial YORP evolution (e.g., Rubincam, 2000; Vokrouhlický and Čapek, 2002).<sup>17</sup> Our computed  $\epsilon$  values for these bodies are testable via lightcurve observations. We caution, however, that several factors may produce large errors in Table 2. For example,  $\epsilon$  values near  $90^\circ$  may be wrong because the transformation from  $\Delta a_p \sim 0^\circ$  to  $\epsilon$  is not well-defined. The best observational strategy is probably to concentrate on Table 2 bodies that have  $\epsilon \sim 0$  or  $\epsilon \sim 180^\circ$ . These  $\epsilon$  values represent our most robust estimates. We found that  $D \gtrsim 3.5$  km members of the Karin cluster are preferentially retrograde rotators. We believe that this result may tell us something about the geometry of the impact event that produced the Karin cluster.

Complications of the above simple interpretation of our results may arise if the Karin cluster asteroids are non-principal axis rotators. Indeed, theoretical studies suggest that the tumbling spin states of km-sized collisional fragments (such as the Karin family members) are not efficiently damped on Myr-timescales by rotational energy dissipation within their interior (Burns and Safronov, 1973; Harris, 1994). The obliquity is ill-defined for tumbling spin states. For a tumbling asteroid, the values of  $\epsilon$  listed in Ta-

ble 2 probably specify the orientation of the spin angular momentum vector. This issue requires further study. In particular, a model of the Yarkovsky effect for tumbling asteroids is not yet available.

Other identified young clusters in the asteroid belt such as the Iannini and Veritas families (Nesvorný et al., 2003) may also be used to constrain non-gravitational effects. We have not used them here because the Iannini cluster does not yet have an unambiguous age, while the Veritas family ( $8.3 \pm 0.05$  Myr old, Nesvorný et al., 2003) is located in a region of the asteroid belt ( $a \sim 3.17$  AU) where many chaotic resonances exist (Milani and Farinella, 1994; Nesvorný and Morbidelli, 1998; Nesvorný et al., 2003). Unfortunately, chaos in the Veritas family region may prohibit us from producing an accurate representation of the past orbital evolutions of member asteroids.

Many of the limitations of our study stem from the fact that only sparse data exists on the physical properties of Karin cluster members. Future observations of these bodies should help to remedy this problem. In particular, observational determinations of albedo, sizes, densities, rotation periods and obliquities of the Karin cluster members using ground-based telescopes together with SIRTf<sup>18</sup> observations should be particularly useful.

## Acknowledgments

This paper is based upon work supported by the NASA Planetary Geology and Geophysics Program under Proposal No. PGG02-0106-0111. We thank David Vokrouhlický and Joseph Spitale for their very helpful referee reports.

## References

- Belton, M.J.S., 19 colleagues, 1994. First images of Asteroid 243 Ida. *Science* 265, 1543–1547.
- Benettin, G., Galgani, L., Strelcyn, J.M., 1976. Kolmogorov entropy and numerical experiments. *Phys. Rev. A* 14, 2338–2345.
- Benz, W., Asphaug, E., 1999. Catastrophic disruptions revisited. *Icarus* 142, 5–20.
- Biesiadecki, J.J., Skeel, R.D., 1993. Dangers of multiple time step methods. *J. Comput. Phys.* 109, 318.
- Binzel, R.P., Xu, S., Bus, S.J., 1993. Spectral variations within the Koronis family—possible implications for the surface colors of Asteroid 243 Ida. *Icarus* 106, 608–611.
- Binzel, R.P., Lupishko, D., di Martino, M., Whiteley, R.J., Hahn, G.J., 2002. Physical properties of near-Earth objects. In: Bottke, W.F., Cellino, A., Paolicchi, P., Binzel, R. (Eds.), *Asteroids III*. Univ. of Arizona Press, Tucson, pp. 255–271.
- Bottke, W.F., Rubincam, D.P., Burns, J.A., 2000. Dynamical evolution of main belt meteoroids: numerical simulations incorporating planetary perturbations and Yarkovsky thermal forces. *Icarus* 145, 301–331.
- Bottke, W.F., Vokrouhlický, D., Brož, M., Nesvorný, D., Morbidelli, A., 2001. Dynamical spreading of asteroid families via the Yarkovsky effect. *Science* 294, 1693–1696.

<sup>17</sup> Using standard theory of the YORP effect (Rubincam, 2000; Vokrouhlický and Čapek, 2002), we estimate that  $\epsilon$  of individual km-sized Karin family members may have changed by  $\lesssim 15^\circ$  over the relevant timescale. For this reason, the original and current obliquities of the Karin family members may differ by several degrees from the ‘average’ values of  $\epsilon$  determined here (Table 1).

<sup>18</sup> <http://sirtf.caltech.edu>.

- Botke, W.F., Vokrouhlický, D., Rubincam, D.P., Brož, M., 2002. The effect of Yarkovsky thermal forces on the dynamical evolution of asteroids and meteoroids. In: Bottke, W.F., Cellino, A., Paolicchi, P., Binzel, R. (Eds.), *Asteroids III*. Univ. of Arizona Press, Tucson, pp. 395–408.
- Bowell, E., Muinonen, K., Wasserman, L.H., 1994. A public-domain asteroid orbit database. In: Milani, A., Di Martino, M., Cellino, A. (Eds.), *Asteroids, Comets and Meteors*. Kluwer, Dordrecht, pp. 477–481.
- Brož, M., 1999. Orbital evolution of asteroid fragments due to planets and thermal effects. Thesis. Charles University, Prague. <http://sirah.troja.mff.cuni.cz/~mira/mp>.
- Burns, J.A., Safronov, V.S., 1973. Asteroid nutation angles. *Mon. Not. R. Astron. Soc.* 165, 403–411.
- Bus, S.J., Binzel, R.P., 2002a. Phase II of the small main-belt asteroid spectroscopic survey. The observations. *Icarus* 158, 106–145.
- Bus, S.J., Binzel, R.P., 2002b. Phase II of the small main-belt asteroid spectroscopic survey. A feature-based taxonomy. *Icarus* 158, 146–177.
- Britt, D.T., Yeomans, D., Housen, K., Consolmagno, G., 2002. Asteroid density, porosity, and structure. In: Bottke, W.F., Cellino, A., Paolicchi, P., Binzel, R. (Eds.), *Asteroids III*. Univ. of Arizona Press, Tucson, pp. 485–500.
- Carruba, V., Burns, J.A., Bottke, W., Nesvorný, D., 2003. Orbital evolution of the Gefion and Adeona asteroid families: close encounters with massive asteroids and the Yarkovsky effect. *Icarus* 162, 308–327.
- Chapman, C.R., Merline, W.J., Thomas, P., 1999. Cratering on Mathilde. *Icarus* 140, 28–33.
- Cheng, A.F., Barnouin-Jha, O.S., 1999. Giant craters on Mathilde. *Icarus* 140, 34–48.
- Chesley, S.R., Ostro, S.J., Vokrouhlický, D., Čapek, D., Giorgini, J.D., Nolan, M.C., Margot, J., Hine, A.A., Benner, L.A.M., Chamberlin, A.B., 2003. Direct detection of the Yarkovsky effect by radar ranging to Asteroid 6489 Golevka. *Science* 302, 1739–1742.
- Dobrovolskis, A.R., Burns, J.A., 1984. Angular momentum drain—a mechanism for despinning asteroids. *Icarus* 57, 464–476.
- Duncan, M.J., Levison, H.F., Lee, M.H., 1998. A multiple time step symplectic algorithm for integrating close encounters. *Astron. J.* 116, 2067–2077.
- Farinella, P., Vokrouhlický, D., 1999. Semimajor axis mobility of asteroidal fragments. *Science* 283, 1507–1510.
- Farinella, P., Vokrouhlický, D., Hartmann, W.K., 1998. Meteorite delivery via Yarkovsky orbital drift. *Icarus* 132, 378–387.
- Harris, A.W., 1994. Tumbling asteroids. *Icarus* 107, 209–211.
- Hilton, J.L., 2002. Asteroid masses and densities. In: Bottke, W.F., Cellino, A., Paolicchi, P., Binzel, R. (Eds.), *Asteroids III*. Univ. of Arizona Press, Tucson, pp. 103–112.
- Jedicke, R., Nesvorný, D., Whiteley, R., Ivezić, Ž., Jurić, M., 2004. An age-colour relationship for main-belt S-complex asteroids. *Nature* 429, 275–277.
- Knežević, Z., Lemaître, A., Milani, A., 2002. The determination of asteroid proper elements. In: Bottke, W.F., Cellino, A., Paolicchi, P., Binzel, R. (Eds.), *Asteroids III*. Univ. of Arizona Press, Tucson, pp. 603–612.
- Laskar, J., 1993. Frequency analysis of a dynamical system. *Celest. Mech. Dynam. Astron.* 56, 191–196.
- Laskar, J., 1995. Frequency map analysis of an Hamiltonian system. In: *Proceedings of Chaos and Diffusion in Hamiltonian systems*, pp. 223–238.
- Levison, H.F., Duncan, M.J., 1994. The long-term dynamical behavior of short-period comets. *Icarus* 108, 18–36.
- Levison, H.F., Duncan, M.J., 2000. Symplectically integrating close encounters with the Sun. *Astron. J.* 120, 2117–2123.
- Love, S.G., Ahrens, T.J., 1997. Origin of asteroid rotation rates in catastrophic impacts. *Nature* 386, 154–156.
- Marzari, F., Davis, D., Vanzani, V., 1995. Collisional evolution of asteroid families. *Icarus* 113, 168–187.
- Michalak, G., 2000. Determination of asteroid masses—I. (1) Ceres, (2) Pallas and (4) Vesta. *Astron. Astrophys.* 360, 363–374.
- Michel, P., Benz, W., Richardson, D.C., 2003. Disruption of fragmented parent bodies as the origin of asteroid families. *Nature* 421, 608–611.
- Milani, A., Farinella, P., 1994. The age of the Veritas asteroid family deduced by chaotic chronology. *Nature* 370, 40–42.
- Milani, A., Knežević, Z., 1994. Asteroid proper elements and the dynamical structure of the asteroid main belt. *Icarus* 107, 219–254.
- Morbidelli, A., Vokrouhlický, D., 2003. The Yarkovsky-driven origin of near-Earth asteroids. *Icarus* 163, 120–134.
- Murray, C.D., Dermott, S.F., 1999. *Solar System Dynamics*. Cambridge Univ. Press, Cambridge.
- Nesvorný, D., Ferraz-Mello, S., 1997a. On the asteroidal population of the first-order jovian resonances. *Icarus* 130, 247–258.
- Nesvorný, D., Ferraz-Mello, S., 1997b. Chaotic diffusion in the 2/1 asteroidal resonance. An application of the frequency map analysis. *Astron. Astrophys.* 320, 672–680.
- Nesvorný, D., Morbidelli, A., 1998. Three-body mean motion resonances and the chaotic structure of the asteroid belt. *Astron. J.* 116, 3029–3037.
- Nesvorný, D., Bottke, W.F., Levison, H., Dones, L., 2002a. A recent asteroid breakup in the main belt. *Nature* 417, 720–722.
- Nesvorný, D., Morbidelli, A., Vokrouhlický, D., Bottke, W.F., Brož, M., 2002b. The Flora family: a case of the dynamically dispersed collisional swarm? *Icarus* 157, 155–172.
- Nesvorný, D., Ferraz-Mello, S., Holman, M., Morbidelli, A., 2002c. Regular and chaotic dynamics in the mean-motion resonances: implications for the structure and evolution of the asteroid belt. In: Bottke, W.F., Cellino, A., Paolicchi, P., Binzel, R. (Eds.), *Asteroids III*. Univ. of Arizona Press, Tucson, pp. 379–394.
- Nesvorný, D., Bottke, W.F., Levison, H.F., Dones, L., 2003. Recent origin of the Solar System dust bands. *Astrophys. J.* 591, 486–497.
- Nesvorný, D., Jedicke, R., Whiteley, R.J., Ivezić, Ž., 2004. Evidence for asteroid space weathering from the Sloan digital sky survey. *Icarus*. Submitted for publication.
- Oseledec, V.I., 1968. A multiplicative ergodic theorem. Lyapunov characteristic numbers for dynamical systems. *Trans. Moscow Math. Soc.* 19, 197–231.
- Pravec, P., Harris, A.W., Michalowski, T., 2002. Asteroid rotations. In: Bottke, W.F., Cellino, A., Paolicchi, P., Binzel, R. (Eds.), *Asteroids III*. Univ. of Arizona Press, Tucson, pp. 113–122.
- Quinlan, G.D., Tremaine, S., 1990. Symmetric multistep methods for the numerical integration of planetary orbits. *Astron. J.* 100, 1694–1700.
- Quinn, T.R., Tremaine, S., Duncan, M., 1991. A three million year integration of the Earth's orbit. *Astron. J.* 101, 2287–2305.
- Rubincam, D.P., 1995. Asteroid orbit evolution due to thermal drag. *J. Geophys. Res.* 100, 1585–1594.
- Rubincam, D.P., 1998. Yarkovsky thermal drag on small asteroids and Mars–Earth delivery. *J. Geophys. Res.* 103, 1725–1732.
- Rubincam, D.P., 2000. Radiative spin-up and spin-down of small asteroids. *Icarus* 148, 2–11.
- Šidlichovský, M., Nesvorný, D., 1997. Frequency modified Fourier transform and its applications to asteroids. *Celest. Mech. Dynam. Astron.* 65, 137–148.
- Šidlichovský, M., Nesvorný, D., 1999. A study of chaos in the asteroid belt. In: *The Dynamics of Small Bodies in the Solar System, A Major Key to Solar System Studies*. In: NATO ASIC Proc., vol. 522, pp. 31–36.
- Spitale, J., Greenberg, R., 2002. Numerical evaluation of the general Yarkovsky effect: effects on eccentricity and longitude of periapease. *Icarus* 156, 211–222.
- Standish, E.M., 1990. The observational basis for JPL's DE 200, the planetary ephemerides of the astronomical almanac. *Astron. Astrophys.* 233, 252–271.
- Tedesco, E.F., Noah, P.V., Noah, M., Price, S.D., 2002. The supplemental IRAS minor planet survey. *Astron. J.* 123, 1056–1085.
- Vokrouhlický, D., 1998a. Diurnal Yarkovsky effect as a source of mobility of meter-sized asteroidal fragments. I. Linear theory. *Astron. Astrophys.* 335, 1093–1100.
- Vokrouhlický, D., 1998b. Diurnal Yarkovsky effect as a source of mobility of meter-sized asteroidal fragments. II. Non-sphericity effects. *Astron. Astrophys.* 338, 353–363.
- Vokrouhlický, D., 1999. A complete linear model for the Yarkovsky thermal force on spherical asteroid fragments. *Astron. Astrophys.* 344, 362–366.

- Vokrouhlický, D., Farinella, P., 2000. Efficient delivery of meteorites to the Earth from a wide range of asteroid parent bodies. *Nature* 407, 606–608.
- Vokrouhlický, D., Čapek, D., 2002. YORP-induced long-term evolution of the spin state of small asteroids and meteoroids: Rubincam's approximation. *Icarus* 159, 449–467.
- Vokrouhlický, D., Brož, M., Farinella, P., Knežević, Z., 2001. Yarkovsky-driven leakage of Koronis family members. *Icarus* 150, 78–93.
- Vokrouhlický, D., Nesvorný, D., Bottke, W.F., 2003. The vector alignments of asteroid spins by thermal torques. *Nature* 425, 147–151.
- Vokrouhlický, D., Chesley, S.R., Čapek, D., Ostro, S.J., 2004. Next Yarkovsky candidates. In: Asteroid Dynamics Workshop. Arecibo Observatory, Puerto Rico, Feb. 2–4.
- Wisdom, J., Holman, M., 1991. Symplectic maps for the  $N$ -body problem. *Astron. J.* 102, 1528–1538.
- Yoshida, F., 16 colleagues, 2004. Photometric observations of Karin family asteroids. In: Asteroid Dynamics Workshop. Arecibo Observatory. Arecibo, Puerto Rico.
- Zappalà, V., Cellino, A., Farinella, P., Knežević, Z., 1990. Asteroid families. I. Identification by hierarchical clustering and reliability assessment. *Astron. J.* 100, 2030–2046.
- Zappalà, V., Cellino, A., Farinella, P., Milani, A., 1994. Asteroid families. II. Extension to unnumbered multiopposition asteroids. *Astron. J.* 107, 772–801.

### Further reading

- Öpik, E.J., 1951. Collision probabilities with the planets and the distribution of interplanetary matter. *Proc. Roy. Irish Acad.* 54, 165–199.